

CERN-EP-2023-268
20 November 2023

Measurements of chemical potentials in Pb–Pb collisions at $\sqrt{s_{\text{NN}}} = 5.02 \text{ TeV}$

ALICE Collaboration*

Abstract

This Letter presents the most precise measurement to date of the matter/antimatter imbalance at midrapidity in Pb–Pb collisions at a center-of-mass energy per nucleon pair $\sqrt{s_{\text{NN}}} = 5.02 \text{ TeV}$. Using the Statistical Hadronization framework, it is possible to obtain the value of the electric charge and baryon chemical potentials, $\mu_Q = -0.18 \pm 0.90 \text{ MeV}$ and $\mu_B = 0.71 \pm 0.45 \text{ MeV}$, with unprecedented precision. A centrality-differential study of the antiparticle-to-particle yield ratios of charged pions, protons, Ω -baryons, and light (hyper)nuclei is performed. These results indicate that the system created in Pb–Pb collisions at the LHC is on average baryon-free and electrically neutral at midrapidity.

*See Appendix D for the list of collaboration members

1 Introduction

Nuclear matter at extremely high energy densities can be generated in the laboratory through relativistic heavy-ion collisions [1–3]. At the LHC, the beam remnants from the collision are located at rapidities $y \approx \pm 6$ and a fraction of the collision energy is deposited at midrapidity [4]. In this region, particles are formed from a nearly baryon number and electric charge free medium. This process can be described in the Color Glass Condensate model via gluon radiation by static quarks, frozen by time dilation [5]. Conversely, string-fragmentation models explain it through the breaking of color flux tubes. Part of the initial baryon number can be transported to midrapidity via either baryon junction formation [6] or di-quark breaking [7]. This phenomenon, known as nuclear stopping, influences the net-baryon density of the system formed at midrapidity [8–10]. The baryon number transport is minimal at the LHC, and the nuclear transparency regime [11] is reached. In this regime, conditions akin to those of the early Universe are replicated, where nearly equal abundances of matter and antimatter were present, as described by the standard cosmological model [12]. Experimentally, one can gauge the extent to which heavy-ion collisions approach the early Universe conditions by measuring the antimatter-to-matter yield ratios across various hadron species.

A comprehensive framework for interpreting these ratios is provided by the Statistical Hadronization Model (SHM)[13–18]. Among the several models that can be used to describe a heavy-ion collision, the SHM is the most successful in describing the yields of all light-flavor hadronic species, which are determined starting from the partition function of the fireball at the freeze-out of inelastic scatterings. This fireball is an equilibrated gas composed of hadrons and resonances (HRG). Due to the substantial particle multiplicity and the finite kinematical acceptance, a Grand Canonical (GC) ensemble description is employed for heavy-ion collisions. In this approach, the conservation of charges, namely the baryon number (B), the electric charge (Q), and strangeness (S), is regulated by the corresponding chemical potentials μ_B , μ_Q , and μ_S , respectively [19, 20]. The baryon chemical potential μ_B represents the net-baryon density of the system, with $\mu_B = 0$ corresponding to an HRG with same amount of baryons and antibaryons. The electric charge potential μ_Q encodes the positive-negative charge imbalance of the gas; it is connected to μ_B by the atomic-to-mass-number ratio Z/A of the colliding ions [21, 22]. The requirement of strangeness neutrality constrains μ_S throughout the entire volume of the fireball [21, 22]. Chemical potentials determine the abundance of hadrons through the fugacity, $\lambda_i = \exp[(B_i\mu_B + Q_i\mu_Q + S_i\mu_S)/T_{\text{ch}}]$, where B_i , Q_i , and S_i denote the quantum numbers of the considered species i , and T_{ch} is the chemical freeze-out temperature, at which hadron yields are determined.

Over the last three decades, the asymmetry between antimatter and matter of the fireball has been systematically studied at different experimental facilities [23–38]. The decreasing trend of μ_B , from about 400 MeV at the SPS to 20 MeV at the top RHIC energy of 200 GeV, and $\mu_B = 0.7 \pm 3.8$ MeV at the LHC is consistent with the decrease of baryon number transport to midrapidity with increasing beam rapidity [36, 37, 39–41]. The formation of baryon number free matter at midrapidity was first reported in pp collisions by ALICE, which observed that the \bar{p}/p yield ratio is compatible with unity [42]. At fixed collision energy, it is also possible to explore nuclear transparency as a function of centrality, i.e., the transverse displacement between the centers of the colliding nuclei, as it affects the dynamics of the colliding nucleons. In particular, a slight increase in μ_B from peripheral to central (head-on) collisions was observed at low energies by STAR at the RHIC beam energy scan [43]. These results were obtained by either comparing the SHM predictions with the measured yields of hadrons and their antimatter counterparts [44] or by directly fitting antiparticle-to-particle yield ratios [39, 43]. The latter method yields more precise results, owing to the cancelation of particle-antiparticle correlated uncertainties and the reduced dependence on model parameters, such as the system volume, V , which is eliminated in the ratios.

In this Letter, we report the most precise estimation to date of μ_B and μ_Q obtained from a set of antiparticle-to-particle yield ratios. The analyzed species are charged pions, protons, Ω^- baryons, and light (hyper)nuclei. (Anti)protons are the most abundantly produced (anti)baryons at midrapidity (≈ 35

and ≈ 2 protons on average in central and peripheral Pb–Pb collisions, respectively [45]). Consequently, the antiproton-to-proton yield ratio can probe the antibaryon-to-baryon imbalance [42, 46] with high precision. On the other hand, the sensitivity to baryon asymmetry is enhanced when light (hyper)nuclei are included because of their larger baryon content. In this work, ${}^3\text{He}$, its isobar ${}^3\text{H}$, and hypertriton ${}^3\Lambda\text{H}$, which is a bound state of a proton, a neutron, and a Λ , along with their antimatter counterparts, are considered¹. The ratio of oppositely charged pions provides a precise constraint on the imbalance of electric charge, as the yield ratio depends predominantly on μ_Q . Finally, the dependence of antimatter-to-matter ratios on strangeness is probed with (anti) Ω^- baryons, which, unlike (anti) Λ and (anti) Ξ^- , have negligible contamination coming from heavier hadron decays.

2 The ALICE detector and data analysis

The results reported in this analysis are obtained from a sample of Pb–Pb collisions at $\sqrt{s_{\text{NN}}} = 5.02$ TeV collected in 2018 by ALICE at the LHC. The ALICE apparatus and its performance are described in detail in Refs. [48, 49]. The minimum-bias collision and centrality triggers are provided by the V0 system [50], which is composed of two arrays of plastic scintillators covering the forward ($2.8 < \eta < 5.1$) and backward ($-3.7 < \eta < -1.7$) regions of pseudorapidity. The coincidence of signals in both detectors determines the minimum bias trigger. The amplitude of the V0 signal is proportional to the charge deposited in the detectors, which is related to the produced charged-particle multiplicity that, in turn, is controlled by the collision centrality. The V0 amplitude is then used to trigger specific categories of central and semicentral events, and to estimate centrality [51]. Five centrality intervals are considered in this Letter, namely 0–5%, 5–10%, 10–30%, 30–50%, and 50–90%, expressed as percentiles of the total hadronic cross section for Pb–Pb collisions. The position of the primary interaction vertex is required to be within a 10 cm wide region centered at the nominal interaction point to profit from the full acceptance of the ALICE central barrel detectors. Events with multiple interaction vertices are rejected to ensure the correct association of reconstructed tracks and primary vertices. The number of events passing these selections is approximately 300 million.

Charged pions, protons, ${}^3\text{He}$, and tritons produced at midrapidity, $|y| < 0.5$, are tracked in the ALICE central barrel: hereafter, charge conjugates are implied unless stated otherwise. The tracks are reconstructed within $|\eta| < 0.8$ and in the full azimuth using the Inner Tracking System (ITS) [52] and the Time Projection Chamber (TPC) [53]. These detectors are placed in a solenoid that provides a uniform magnetic field of 0.5 T parallel to the beam axis. The antiparticle-to-particle yield ratios are measured as a function of the transverse momentum p_T in the ranges $0.7 \leq p_T < 1.6$ GeV/ c for π^-/π^+ , $0.5 \leq p_T < 3$ GeV/ c for \bar{p}/p , $1.6 \leq p_T < 3$ GeV/ c for ${}^3\bar{\text{H}}/{}^3\text{H}$, and $2 \leq p_T < 8$ GeV/ c for ${}^3\bar{\text{He}}/{}^3\text{He}$ to select the bulk of the production and ensure good identification performance.

The analysis procedure for extracting particle yields is similar to the one adopted in previous analyses [45, 54, 55]. Standard selections on the χ^2 of the track fit, on the number of reconstructed track points in the ITS and the TPC, and on the distance of closest approach (DCA) of the extrapolation of the track to the primary interaction vertex ensure a good reconstruction of tracks originating from the collisions. Particle identification (PID) is performed on a statistical basis by measuring the specific energy loss (dE/dx) in both the TPC and the ITS, and particle velocity depending on the transverse momentum of the measured particles with the Time-Of-Flight detector (TOF). Further details about the PID are provided in the appendix A.1.

The residual contamination due to hyperon weak decays and spallation reactions of primary particles in the apparatus is evaluated by fitting the measured DCA distribution in the plane transverse to the beam axis with templates computed via Monte Carlo (MC) simulations for the various processes in-

¹(Anti)deuterons, d/\bar{d} are not considered in this Letter since the efficiency correction for \bar{d} is based on the \bar{d} absorption cross section extracted by the ALICE Collaboration from the measured \bar{d}/d yield ratio itself [47].

volved [45, 54, 55]. The extracted yields are corrected for the detector acceptance and candidate selection efficiency, computed using MC simulations, as the fraction of particles reconstructed out of all MC-generated primary particles. The Pb–Pb event is generated with HIJING [56], while the particles are transported through a realistic model of the ALICE apparatus with GEANT4 [57]. To increase the simulated sample size protons, ${}^3\text{He}$ nuclei, and tritons are injected on top of each HIJING event. The available measurements of hadron inelastic cross sections are used to correct the GEANT4 parameterizations of the corresponding reactions [58–72].

The ${}^3\Lambda\text{H}$ candidates are reconstructed from their two-body charged mesonic decay ${}^3\Lambda\text{H} \rightarrow {}^3\text{He} + \pi^-$. The reconstruction algorithm is the same as the one applied in previous measurements [73–76]. The Ω^- is reconstructed with a similar procedure from the decay into a charged kaon and a Λ baryon, that, in turn, is reconstructed from its charged two-body decay, $\Omega^- \rightarrow K^- + \Lambda(\rightarrow \pi^- + p)$ [77–79]. The ratios are extracted in intervals of proper decay length $ct = cML/p$, with M , L , and p being the mass, trajectory length, and candidate momentum, respectively. In particular, $2 \leq ct < 35$ cm for ${}^3\Lambda\text{H}$ and $1 \leq ct < 10$ cm for Ω^- are used. The ${}^3\Lambda\text{H}$ and Ω^- candidates are selected with Boosted Decision Tree (BDT) algorithms [80], which are applied on top of preliminary kinematic and topological selections to enhance the background rejection. The BDT internal parameters and selections are optimized using samples of correctly classified signal and background candidates, as explained in detail in the appendix A.2.

The invariant mass distribution of the selected candidates is fitted with a probability density function built with a Kernel Density Estimation (KDE) [81, 82] in the MC for ${}^3\Lambda\text{H}$, whereas an extended Crystal-Ball function is used for the Ω^- signal [83]. An exponential function is used to model the residual background in both cases. The yields extracted as the integral of the signal functions obtained from the fits are corrected by the overall selection efficiency and acceptance computed in the MC simulations. As in previous ${}^3\Lambda\text{H}$ analyses [76], an absorption correction factor is included to account for undetected candidates absorbed in the detector material before their decay.

The following systematic uncertainty contributions are estimated for the antiparticle-to-particle yield ratios: candidate selection and signal extraction, MC data sample size, material budget uncertainty, absorption cross section uncertainties, and magnetic field polarity. The details about the estimation and values of such contributions are reported in the appendix A.3.

3 Results

The fully corrected antiparticle-to-particle yield ratios do not exhibit any significant dependence on p_T and ct (see Fig. A.1 appendix A.4). This observation, which is consistent across particle species and centrality intervals, implies that the production spectra of charge-conjugate species only differ by normalization factors proportional to their yields. The antiparticle-to-particle yield ratios of each species are obtained as the averages weighted with the total uncorrelated uncertainties of the p_T - and ct -differential ratios in each centrality interval. For ${}^3\Lambda\text{H}$, no statistically significant signal is observed in the 50–90% centrality range.

The chemical potentials μ_B and μ_Q are extracted by fitting the antiparticle-to-particle yield ratios with the predictions of the GC statistical hadronization model using the Thermal-FIST code [22]. The measured ratios and the SHM fit results are reported in Fig. 1. The chemical freeze-out temperature is set to $T_{\text{ch}} = 155 \pm 2$ MeV, as obtained from a fit to the ALICE data [84, 85]: its value is compatible with the pseudo-critical temperature extracted with lattice QCD calculations [86]. This value is fixed for all centralities, since in heavy-ion collisions only a mild dependence of T_{ch} on centrality is observed (less than 3% [43, 84]); additionally, antiparticle-to-particle yield ratios show a negligible dependence on T_{ch} for $\mu_B \approx 1$ MeV [44]. The uncertainty on T_{ch} , which is compatible with the range of variations of T_{ch} observed as a function of centrality, is considered as a centrality-correlated source of systematic uncertainty. The strangeness chemical potential μ_S is constrained in the fit from strangeness conservation.

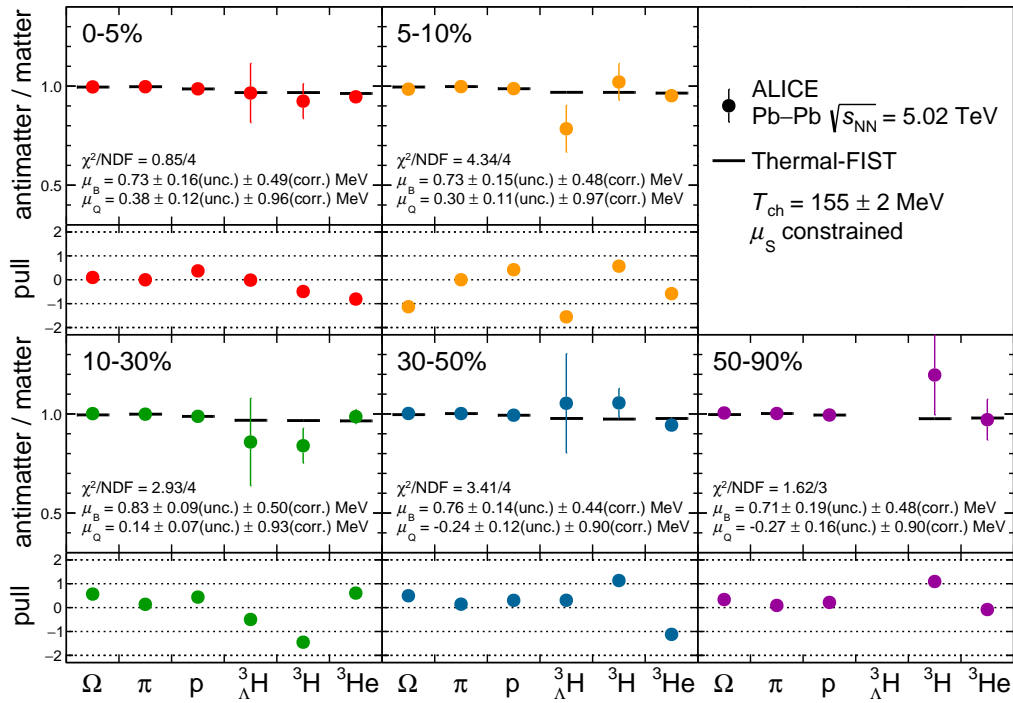


Figure 1: Upper panels: statistical hadronization model fits to the measured antiparticle-to-particle yield ratios in different centrality intervals. Error bars show the sum in quadrature of statistical and centrality-uncorrelated systematic uncertainties. When not visible, error bars are hidden by the marker. Lower panels: pull distribution, defined as the difference between data and fit values, normalized to the uncertainty in the data.

The contribution of strongly-decaying resonances is accounted in the model predictions as it cannot be directly disentangled in the data. For the χ^2 minimization, the quadratic sum of statistical and uncorrelated systematic uncertainty is considered. The effect of the centrality-correlated sources is evaluated by repeating the fit to ratios coherently increased or decreased by their uncertainties. The uncertainty assigned to μ_B and μ_Q is half of the deviation between the results obtained in the two cases.

In this Letter, yield ratios are analyzed within the GC statistical model also in the most peripheral events, where canonical ensemble formulation is needed for an accurate description of hadron yields by requiring exact conservation of charges over a finite volume [87, 88]. It is known, however, that effects connected to the canonical conservation of charges cancel out when considering antiparticle-to-particle yield ratios, and their values are well described by the GC ensemble [15, 89]. Indeed, good fit quality is obtained across the 0-90% centrality range using the GC model to quantify these ratios. In addition, the yield ratio $\bar{\Omega}^+/\Omega^-$ is compatible with unity as expected in the SHM, where it is independent of μ_B and μ_S for $\mu_B \sim 0$ [16].

The chemical potentials obtained in different centrality intervals are shown in the left panel of Fig. 2. The centrality dependence of μ_B and μ_Q is studied by fitting independently the centrality-differential μ_B and μ_Q results with a constant function, taking into account the full correlation matrix of the measurements, which are reported in appendix B. The χ^2 profiles of the fits are reported in appendix C.1. The fit probability is $P = 0.97$ for μ_B and $P = 0.64$ for μ_Q : therefore, no evidence of centrality dependence is found, even if a larger μ_B would be expected in more central collisions due to a potentially larger baryon stopping [4]. The fit of the centrality-differential values yields chemical potentials $\mu_B = 0.71 \pm 0.45$ MeV and $\mu_Q = -0.18 \pm 0.90$ MeV, which are compatible with zero within 1.6σ and 0.2σ , respectively. The comparison with the previous data point of μ_B at the LHC [35–38] shows a significant improvement in the

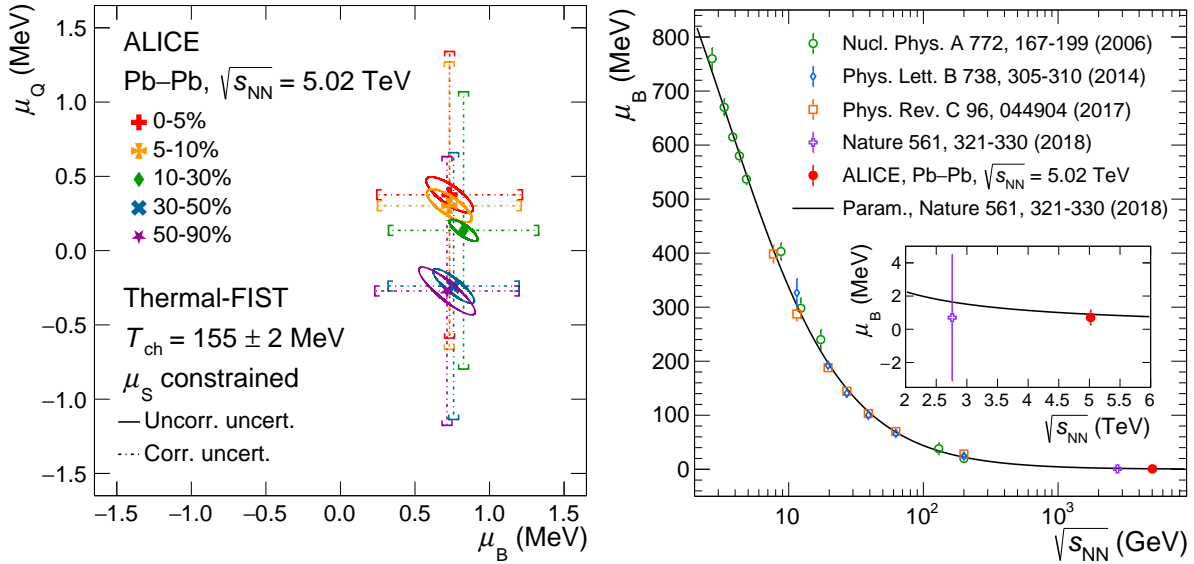


Figure 2: Left panel: μ_B and μ_Q obtained with Thermal-FIST [22] in different centrality intervals. The centrality-correlated and -uncorrelated uncertainties are represented with error bars and ellipses, respectively. Right panel: μ_B extracted from data collected in Au–Au and Pb–Pb collisions at the AGS (E802, E866, E877, E895, E896, E917 Collaborations), SPS (NA44, NA49, NA47 Collaborations), RHIC (BRAHMS, PHENIX, STAR Collaboration), and LHC (ALICE Collaboration) as a function of the center-of-mass energy per nucleon–nucleon pair [39, 41, 43], and phenomenological parameterization of $\mu_B(\sqrt{s_{\text{NN}}})$ [36]. The inset shows more in detail the results obtained at the LHC [36].

precision by a factor larger than eight (no direct value of μ_Q was provided in that study, see below). These results imply that the system created at midrapidity in Pb–Pb collisions is baryon- and electrically-neutral on average. As a consequence, this observation shows that the nuclear transparency regime is reached, i.e., baryon transport from the colliding ions to the interaction region is negligible. Due to the absence of any centrality dependence, it is also concluded that nuclear transparency is achieved even in central Pb–Pb collisions, where a larger-than-zero μ_B could be expected from a more significant baryon number transport at midrapidity.

As a cross check, the SHM fits described above are repeated by also constraining μ_Q from initial conditions via conservation laws, as it was done also in past measurements [36, 39, 43]. Specifically, the μ_Q/μ_B ratio is fixed by requiring that the average charge-to-baryon density ratio of the created hadron system, $\langle n_Q \rangle / \langle n_B \rangle$, is equivalent to the Z/A ratio of colliding nuclei, i.e., $\langle n_Q \rangle / \langle n_B \rangle = Z/A \approx 0.4$ for ^{208}Pb [21]. The μ_B values extracted from the fits in each centrality interval are successfully fitted with a constant function (fit probability $P = 0.09$). The resulting μ_B value is compatible with the one reported above within uncertainties. Similar results are obtained by fitting the antiparticle-to-particle yield ratios using the GSI-Heidelberg model [15, 37, 39], with $T_{\text{ch}} = 156.6 \pm 1.7$ MeV [38] and μ_Q is fixed to initial conditions: the average value across centrality is $\mu_B = 0.90 \pm 0.43$ MeV. The χ^2 profile of the fit is reported in appendix C.2. Using the values of μ_B and μ_Q extracted in the 5% most central collisions, the inclusive net-proton density at midrapidity, $2/\langle N_{\text{part}} \rangle dN_{\text{p}-\bar{\text{p}}}/dy$, can be computed in the SHM framework. The value extracted with Thermal-FIST is $(3.4 \pm 1.4) \times 10^{-3}$, while using the GSI-Heidelberg model, a value of $5.9^{+2.2}_{-2.8} \times 10^{-3}$ is obtained. In both cases, the obtained results agree with the exponential trend as a function of beam rapidity predicted by the baryon-junction mechanism [90].

The right panel of Fig. 2 shows the comparison of the current with past estimations of μ_B as a function of the center-of-mass energy of the collision [36, 39, 41, 43]. The comparison with the previous LHC data point is highlighted in the inset of the figure. The result reported in this Letter is compatible with the

extrapolation of the phenomenological parameterization based on previous data and reported in Ref. [36].

4 Conclusions

In summary, the most precise measurement of the asymmetry between matter and antimatter at the LHC is reported in this Letter. The asymmetry is quantified through antiparticle-to-particle yield ratios of different hadrons, which are analyzed within the statistical hadronization framework to extract the chemical potentials μ_B and μ_Q . The GC version of the model accurately describes the antiparticle-to-particle yield ratios across centrality, indicating the elimination of effects from canonical charge conservation in peripheral events. The cancelation of correlated uncertainties in these ratios leads to a significant improvement in the μ_B precision: the uncertainty on the obtained value is about one order of magnitude smaller than the previously published one [36]. In addition, a direct estimation of μ_Q is provided. Furthermore, the first centrality-differential study of chemical potentials at the LHC is reported in this Letter. The obtained chemical potentials are consistent with zero, i.e., with the nuclear transparency regime being reached across the full centrality range, thus indicating that baryon transport to midrapidity is negligible even in the most central events at the LHC. The results reported in this Letter show with unprecedented precision that the medium created in heavy-ion collisions at the LHC approaches the early Universe conditions more than any other experimental facility.

Acknowledgements

The ALICE Collaboration would like to thank all its engineers and technicians for their invaluable contributions to the construction of the experiment and the CERN accelerator teams for the outstanding performance of the LHC complex. The ALICE Collaboration gratefully acknowledges the resources and support provided by all Grid centres and the Worldwide LHC Computing Grid (WLCG) collaboration. The ALICE Collaboration acknowledges the following funding agencies for their support in building and running the ALICE detector: A. I. Alikhanyan National Science Laboratory (Yerevan Physics Institute) Foundation (ANSL), State Committee of Science and World Federation of Scientists (WFS), Armenia; Austrian Academy of Sciences, Austrian Science Fund (FWF): [M 2467-N36] and Nationalstiftung für Forschung, Technologie und Entwicklung, Austria; Ministry of Communications and High Technologies, National Nuclear Research Center, Azerbaijan; Conselho Nacional de Desenvolvimento Científico e Tecnológico (CNPq), Financiadora de Estudos e Projetos (Finep), Fundação de Amparo à Pesquisa do Estado de São Paulo (FAPESP) and Universidade Federal do Rio Grande do Sul (UFRGS), Brazil; Bulgarian Ministry of Education and Science, within the National Roadmap for Research Infrastructures 2020-2027 (object CERN), Bulgaria; Ministry of Education of China (MOEC) , Ministry of Science & Technology of China (MSTC) and National Natural Science Foundation of China (NSFC), China; Ministry of Science and Education and Croatian Science Foundation, Croatia; Centro de Aplicaciones Tecnológicas y Desarrollo Nuclear (CEADEN), Cubaenergía, Cuba; Ministry of Education, Youth and Sports of the Czech Republic, Czech Republic; The Danish Council for Independent Research | Natural Sciences, the VILLUM FONDEN and Danish National Research Foundation (DNRF), Denmark; Helsinki Institute of Physics (HIP), Finland; Commissariat à l’Energie Atomique (CEA) and Institut National de Physique Nucléaire et de Physique des Particules (IN2P3) and Centre National de la Recherche Scientifique (CNRS), France; Bundesministerium für Bildung und Forschung (BMBF) and GSI Helmholtzzentrum für Schwerionenforschung GmbH, Germany; General Secretariat for Research and Technology, Ministry of Education, Research and Religions, Greece; National Research, Development and Innovation Office, Hungary; Department of Atomic Energy Government of India (DAE), Department of Science and Technology, Government of India (DST), University Grants Commission, Government of India (UGC) and Council of Scientific and Industrial Research (CSIR), India; National Research and Innovation Agency - BRIN, Indonesia; Istituto Nazionale di Fisica Nucleare (INFN), Italy; Japanese Ministry of Education, Culture, Sports, Science and Technology (MEXT) and Japan Society

for the Promotion of Science (JSPS) KAKENHI, Japan; Consejo Nacional de Ciencia (CONACYT) y Tecnología, through Fondo de Cooperación Internacional en Ciencia y Tecnología (FONCICYT) and Dirección General de Asuntos del Personal Académico (DGAPA), Mexico; Nederlandse Organisatie voor Wetenschappelijk Onderzoek (NWO), Netherlands; The Research Council of Norway, Norway; Commission on Science and Technology for Sustainable Development in the South (COMSATS), Pakistan; Pontificia Universidad Católica del Perú, Peru; Ministry of Education and Science, National Science Centre and WUT ID-UB, Poland; Korea Institute of Science and Technology Information and National Research Foundation of Korea (NRF), Republic of Korea; Ministry of Education and Scientific Research, Institute of Atomic Physics, Ministry of Research and Innovation and Institute of Atomic Physics and Universitatea Națională de Știință și Tehnologie Politehnica București, Romania; Ministry of Education, Science, Research and Sport of the Slovak Republic, Slovakia; National Research Foundation of South Africa, South Africa; Swedish Research Council (VR) and Knut & Alice Wallenberg Foundation (KAW), Sweden; European Organization for Nuclear Research, Switzerland; Suranaree University of Technology (SUT), National Science and Technology Development Agency (NSTDA) and National Science, Research and Innovation Fund (NSRF via PMU-B B05F650021), Thailand; National Academy of Sciences of Ukraine, Ukraine; Science and Technology Facilities Council (STFC), United Kingdom; National Science Foundation of the United States of America (NSF) and United States Department of Energy, Office of Nuclear Physics (DOE NP), United States of America. In addition, individual groups or members have received support from: European Research Council, Strong 2020 - Horizon 2020 (grant nos. 950692, 824093), European Union; Academy of Finland (Center of Excellence in Quark Matter) (grant nos. 346327, 346328), Finland.

References

- [1] E. Shuryak, “Strongly coupled quark-gluon plasma in heavy ion collisions”, *Rev. Mod. Phys.* **89** (2017) 035001, arXiv:1412.8393 [hep-ph].
- [2] P. Braun-Munzinger, V. Koch, T. Schäfer, and J. Stachel, “Properties of hot and dense matter from relativistic heavy ion collisions”, *Phys. Rept.* **621** (2016) 76–126, arXiv:1510.00442 [nucl-th].
- [3] W. Busza, K. Rajagopal, and W. van der Schee, “Heavy Ion Collisions: The Big Picture, and the Big Questions”, *Ann. Rev. Nucl. Part. Sci.* **68** (2018) 339–376, arXiv:1802.04801 [hep-ph].
- [4] Y. Mehtar-Tani and G. Wolschin, “Baryon stopping and saturation physics in relativistic collisions”, *Phys. Rev. C* **80** (2009) 054905, arXiv:0907.5444 [hep-ph].
- [5] L. D. McLerran and R. Venugopalan, “Computing quark and gluon distribution functions for very large nuclei”, *Phys. Rev. D* **49** (1994) 2233–2241, arXiv:hep-ph/9309289.
- [6] S. E. Vance, M. Gyulassy, and X. N. Wang, “Baryon junction stopping at the SPS and RHIC via HIJING/B”, *Nucl. Phys. A* **638** (1998) 395C–398C, arXiv:nucl-th/9802036.
- [7] A. Capella and B. Z. Kopeliovich, “Novel mechanism of nucleon stopping in heavy ion collisions”, *Phys. Lett. B* **381** (1996) 325–330, arXiv:hep-ph/9603279.
- [8] F. Videbaek, “Stopping and baryon transport in heavy ion reactions”, *J. Phys. Conf. Ser.* **50** (2006) 134–141, arXiv:nucl-ex/0505010.
- [9] V. Topor Pop, J. Barrette, C. Gale, S. Jeon, and M. Gyulassy, “Stopping Power from SPS to LHC energies”, arXiv:0705.2759 [hep-ph].
- [10] J. Hoelck and G. Wolschin, “Baryon stopping as a relativistic Markov process in phase space”, *Phys. Rev. Res.* **2** (2020) 033409, arXiv:2009.08913 [nucl-th].

- [11] H. Elfner and B. Müller, “The exploration of hot and dense nuclear matter: introduction to relativistic heavy-ion physics”, *J. Phys. G* **50** (2023) 103001, arXiv:2210.12056 [nucl-th].
- [12] M. J. Fromerth, I. Kuznetsova, L. Labun, J. Letessier, and J. Rafelski, “From Quark-Gluon Universe to Neutrino Decoupling: $200 < T < 2\text{MeV}$ ”, *Acta Phys. Polon. B* **43** (2012) 2261–2284, arXiv:1211.4297 [nucl-th].
- [13] P. Braun-Munzinger and J. Stachel, “Dynamics of ultrarelativistic nuclear collisions with heavy beams: An Experimental overview”, *Nucl. Phys. A* **638** (1998) 3–18, arXiv:nucl-ex/9803015.
- [14] J. Cleymans and K. Redlich, “Unified description of freezeout parameters in relativistic heavy ion collisions”, *Phys. Rev. Lett.* **81** (1998) 5284–5286, arXiv:nucl-th/9808030.
- [15] P. Braun-Munzinger, K. Redlich, and J. Stachel, “Particle production in heavy ion collisions”, in *Quark–Gluon Plasma 3*, pp. 491–599. World Scientific, 2004. arXiv:nucl-th/0304013.
- [16] J. Cleymans, H. Oeschler, K. Redlich, and S. Wheaton, “Comparison of chemical freeze-out criteria in heavy-ion collisions”, *Phys. Rev. C* **73** (2006) 034905, arXiv:hep-ph/0511094.
- [17] P. Braun-Munzinger and J. Wambach, “The Phase Diagram of Strongly-Interacting Matter”, *Rev. Mod. Phys.* **81** (2009) 1031–1050, arXiv:0801.4256 [hep-ph].
- [18] V. Vovchenko and H. Stoecker, “Examination of the sensitivity of the thermal fits to heavy-ion hadron yield data to the modeling of the eigenvolume interactions”, *Phys. Rev. C* **95** (2017) 044904, arXiv:1606.06218 [hep-ph].
- [19] R. Hagedorn and K. Redlich, “Statistical Thermodynamics in Relativistic Particle and Ion Physics: Canonical or Grand Canonical?”, *Z. Phys. C* **27** (1985) 541.
- [20] K. Redlich, J. Cleymans, H. Oeschler, and A. Tounsi, “Conservation laws and particle production in heavy ion collisions”, *AIP Conf. Proc.* **594** (2002) 318–329, arXiv:hep-ph/0110337.
- [21] A. Bazavov *et al.*, “Freeze-out Conditions in Heavy Ion Collisions from QCD Thermodynamics”, *Phys. Rev. Lett.* **109** (2012) 192302, arXiv:1208.1220 [hep-lat].
- [22] V. Vovchenko and H. Stoecker, “Thermal-FIST: A package for heavy-ion collisions and hadronic equation of state”, *Comput. Phys. Commun.* **244** (2019) 295–310, arXiv:1901.05249 [nucl-th].
- [23] J. Stachel and P. Braun-Munzinger, “Stopping in High-energy Nucleus Nucleus Collisions: Analysis in the Landau Hydrodynamic Model”, *Phys. Lett. B* **216** (1989) 1–6.
- [24] P. Braun-Munzinger, J. Stachel, J. P. Wessels, and N. Xu, “Thermal equilibration and expansion in nucleus-nucleus collisions at the AGS”, *Phys. Lett. B* **344** (1995) 43–48, arXiv:nucl-th/9410026.
- [25] **E802** Collaboration, L. Ahle *et al.*, “Anti-proton production in Au + Au collisions at 11.7 AGeV/c”, *Phys. Rev. Lett.* **81** (1998) 2650–2654, arXiv:nucl-ex/9709005.
- [26] **NA49** Collaboration, F. Siklér *et al.*, “Hadron production in nuclear collisions from the NA49 experiment at 158 GeV/c/A”, *Nucl. Phys. A* **661** (1999) 45–54.
- [27] P. Braun-Munzinger, I. Heppe, and J. Stachel, “Chemical equilibration in Pb + Pb collisions at the SPS”, *Phys. Lett. B* **465** (1999) 15–20, arXiv:nucl-th/9903010.

- [28] F. Becattini, J. Cleymans, A. Keranen, E. Suhonen, and K. Redlich, “Features of particle multiplicities and strangeness production in central heavy ion collisions between 1.7 AGeV/c and 158 AGeV/c”, *Phys. Rev. C* **64** (2001) 024901, arXiv:hep-ph/0002267.
- [29] P. Braun-Munzinger and J. Stachel, “Particle ratios, equilibration, and the QCD phase boundary”, *J. Phys. G* **28** (2002) 1971–1976, arXiv:nucl-th/0112051.
- [30] **STAR** Collaboration, C. Adler *et al.*, “Midrapidity anti-proton to proton ratio from Au + Au collisions at $\sqrt{s_{\text{NN}}} = 130$ GeV”, *Phys. Rev. Lett.* **86** (2001) 4778, arXiv:nucl-ex/0104022. [Erratum: Phys.Rev.Lett. 90, 119903 (2003)].
- [31] **BRAHMS** Collaboration, I. G. Bearden *et al.*, “Rapidity dependence of anti-proton to proton ratios in Au+A collisions at $\sqrt{s_{\text{NN}}} = 130$ GeV”, *Phys. Rev. Lett.* **87** (2001) 112305, arXiv:nucl-ex/0106011.
- [32] P. Braun-Munzinger, D. Magestro, K. Redlich, and J. Stachel, “Hadron production in Au - Au collisions at RHIC”, *Phys. Lett. B* **518** (2001) 41–46, arXiv:hep-ph/0105229.
- [33] D. Magestro, “Evidence for chemical equilibration at RHIC”, *J. Phys. G* **28** (2002) 1745–1752, arXiv:hep-ph/0112178.
- [34] F. Becattini, M. Gazdzicki, A. Keranen, J. Manninen, and R. Stock, “Chemical equilibrium in nucleus nucleus collisions at relativistic energies”, *Phys. Rev. C* **69** (2004) 024905, arXiv:hep-ph/0310049.
- [35] **ALICE** Collaboration, B. Abelev *et al.*, “Centrality dependence of π , K, p production in Pb-Pb collisions at $\sqrt{s_{\text{NN}}} = 2.76$ TeV”, *Phys. Rev. C* **88** (2013) 044910, arXiv:1303.0737 [hep-ex].
- [36] A. Andronic, P. Braun-Munzinger, K. Redlich, and J. Stachel, “Decoding the phase structure of QCD via particle production at high energy”, *Nature* **561** (2018) 321–330, arXiv:1710.09425 [nucl-th].
- [37] A. Andronic, P. Braun-Munzinger, B. Friman, P. M. Lo, K. Redlich, and J. Stachel, “The thermal proton yield anomaly in Pb-Pb collisions at the LHC and its resolution”, *Phys. Lett. B* **792** (2019) 304–309, arXiv:1808.03102 [hep-ph].
- [38] A. Andronic, P. Braun-Munzinger, K. Redlich, and J. Stachel, “Hadron yields in central nucleus-nucleus collisions, the statistical hadronization model and the QCD phase diagram”, in *Criticality in QCD and the Hadron Resonance Gas*. 1, 2021. arXiv:2101.05747 [nucl-th].
- [39] A. Andronic, P. Braun-Munzinger, and J. Stachel, “Hadron production in central nucleus-nucleus collisions at chemical freeze-out”, *Nucl. Phys. A* **772** (2006) 167–199, arXiv:nucl-th/0511071.
- [40] A. Andronic, P. Braun-Munzinger, and J. Stachel, “Thermal hadron production in relativistic nuclear collisions: The Hadron mass spectrum, the horn, and the QCD phase transition”, *Phys. Lett. B* **673** (2009) 142–145, arXiv:0812.1186 [nucl-th]. [Erratum: Phys.Lett.B 678, 516 (2009)].
- [41] P. Alba, W. Alberico, R. Bellwied, M. Bluhm, V. Mantovani Sarti, M. Nahrgang, and C. Ratti, “Freeze-out conditions from net-proton and net-charge fluctuations at RHIC”, *Phys. Lett. B* **738** (2014) 305–310, arXiv:1403.4903 [hep-ph].
- [42] **ALICE** Collaboration, K. Aamodt *et al.*, “Midrapidity antiproton-to-proton ratio in pp collisions at $\sqrt{s} = 0.9$ and 7 TeV measured by the ALICE experiment”, *Phys. Rev. Lett.* **105** (2010) 072002, arXiv:1006.5432 [hep-ex].

- [43] **STAR** Collaboration, L. Adamczyk *et al.*, “Bulk Properties of the Medium Produced in Relativistic Heavy-Ion Collisions from the Beam Energy Scan Program”, *Phys. Rev. C* **96** (2017) 044904, arXiv:1701.07065 [nucl-ex].
- [44] J. Cleymans, I. Kraus, H. Oeschler, K. Redlich, and S. Wheaton, “Statistical model predictions for particle ratios at $\sqrt{s_{\text{NN}}} = 5.5$ TeV”, *Phys. Rev. C* **74** (2006) 034903, arXiv:hep-ph/0604237.
- [45] **ALICE** Collaboration, S. Acharya *et al.*, “Production of charged pions, kaons, and (anti-)protons in Pb-Pb and inelastic $p p$ collisions at $\sqrt{s_{\text{NN}}} = 5.02$ TeV”, *Phys. Rev. C* **101** (2020) 044907, arXiv:1910.07678 [nucl-ex].
- [46] **ALICE** Collaboration, E. Abbas *et al.*, “Mid-rapidity anti-baryon to baryon ratios in pp collisions at $\sqrt{s} = 0.9, 2.76$ and 7 TeV measured by ALICE”, *Eur. Phys. J. C* **73** (2013) 2496, arXiv:1305.1562 [nucl-ex].
- [47] **ALICE** Collaboration, S. Acharya *et al.*, “Measurement of the low-energy antideuteron inelastic cross section”, *Phys. Rev. Lett.* **125** (2020) 162001, arXiv:2005.11122 [nucl-ex].
- [48] **ALICE** Collaboration, K. Aamodt *et al.*, “The ALICE experiment at the CERN LHC”, *JINST* **3** (2008) S08002.
- [49] **ALICE** Collaboration, B. B. Abelev *et al.*, “Performance of the ALICE Experiment at the CERN LHC”, *Int. J. Mod. Phys. A* **29** (2014) 1430044, arXiv:1402.4476 [nucl-ex].
- [50] **ALICE** Collaboration, E. Abbas *et al.*, “Performance of the ALICE VZERO system”, *JINST* **8** (2013) P10016, arXiv:1306.3130 [nucl-ex].
- [51] **ALICE** Collaboration, “Centrality determination in heavy ion collisions”, *ALICE-PUBLIC-2018-011* (2018) . <https://cds.cern.ch/record/2636623>.
- [52] **ALICE** Collaboration, K. Aamodt *et al.*, “Alignment of the ALICE Inner Tracking System with cosmic-ray tracks”, *JINST* **5** (2010) P03003, arXiv:1001.0502 [physics.ins-det].
- [53] J. Alme *et al.*, “The ALICE TPC, a large 3-dimensional tracking device with fast readout for ultra-high multiplicity events”, *Nucl. Instrum. Meth. A* **622** (2010) 316–367, arXiv:1001.1950 [physics.ins-det].
- [54] **ALICE** Collaboration, J. Adam *et al.*, “Production of light nuclei and anti-nuclei in pp and Pb-Pb collisions at energies available at the CERN Large Hadron Collider”, *Phys. Rev. C* **93** (2016) 024917, arXiv:1506.08951 [nucl-ex].
- [55] **ALICE** Collaboration, S. Acharya *et al.*, “Light (anti)nuclei production in Pb-Pb collisions at $\sqrt{s_{\text{NN}}} = 5.02$ TeV”, *Phys. Rev. C* **107** (2023) 064904, arXiv:2211.14015 [nucl-ex].
- [56] X.-N. Wang and M. Gyulassy, “HIJING: A Monte Carlo model for multiple jet production in p p, p A and A A collisions”, *Phys. Rev. D* **44** (1991) 3501–3516.
- [57] **GEANT4** Collaboration, S. Agostinelli *et al.*, “GEANT4—a simulation toolkit”, *Nucl. Instrum. Meth. A* **506** (2003) 250–303.
- [58] F. F. Chen, C. P. Leavitt, and A. M. Shapiro, “Attenuation Cross Sections for 860-Mev Protons”, *Physical Review* **99** (1955) 857.
- [59] N. E. Booth, B. Ledley, D. Walker, and D. H. White, “Nuclear cross sections for 900 MeV protons.”, *Proc. Physical Society (London), Section A* **70** (1957) 209.

- [60] N. T. Porile, “Simple Nuclear Reactions of Indium with 30 and 2.9 GeV Protons”, *Physical Review* **128** (1962) 1916.
- [61] O. Artun, *et al.*, “Multinucleon Removal Induced by High-Energy Protons”, *Phys. Rev. Lett.* **35** (1975) 773.
- [62] M. E. Sadler, P. P. Singh, J. Jastrzebski, L. L. Rutledge, J. , and R. E. Segel, “Interaction of 80-164 MeV Protons with Nickel Isotopes”, *Phys. Rev. C* **21** (1980) 2303.
- [63] D. Ashery, I. Navon, G. Azuelos, H. K. Walter, H. J. Pfeiffer, and F. W. Schleputz, “True Absorption and Scattering of Pions on Nuclei”, *Phys. Rev. C* **23** (1981) 2173–2185.
- [64] K. Nakamura, J. Chiba, T. Fujii, H. Iwasaki, T. Kageyama, S. Kurabayashi, T. Sumiyoshi, T. Takeda, H. Ikeda, and Y. Takada, “Absorption and Forward Scattering of Antiprotons by C, Al, and Cu Nuclei in the Region 470-880 MeV/c”, *Phys. Rev. Lett.* **52** (1984) 731–734.
- [65] J. A. McGill, G. W. Hoffmann, M. L. Barlett, R. W. Fergerson, E. C. Milner, R. E. Chrien, R. J. Sutter, T. Kozlowski, and R. L. Stearns, “Proton + Nucleus Inclusive (p,p') Scattering at 800 MeV”, *Phys. Rev. C* **29** (1984) 204.
- [66] N. G. Zaitseva, E. Rurarz, M. Vobecky, K. H. Hwan, K. Nowak, T. Tethal, V. A. Khalkin, and L. M. Popinenkova, “Excitation Function and Yield for ^{97}Ru Production in $^{99}\text{Tc}(\text{p},\text{3n})^{97}\text{Ru}$ Reaction in 20-100 MeV Proton Energy Range”, *Radiochimica Acta* **56** (1992) 59.
- [67] V. F. Kuzichev, Y. B. Lepikhin, and V. A. Smirnitsky, “The Anti-proton - nuclei annihilation cross-section at the momentum range from 0.70 GeV/c to 2.5 GeV/c”, *Nucl. Phys. A* **576** (1994) 581–602.
- [68] C. M. Herbach, *et al.*, “Systematic investigation of 1.2 GeV proton-induced spallation reactions on targets between Al and U”, *Nucl. Instrum. Methods in Physics Res., Sect.A* **562** (2006) 729.
- [69] M. Zamani, S. Stoulos, M. Fragopoulou, M. Manolopoulou, and M. Krivopustov, “Indirect measurement of inelastic cross section of relativistic protons in Pb target”, *Annals of Nuclear Energy* **37** (2010) 923.
- [70] D. W. Bardayan, *et al.*, “Inelastic $^{17}\text{F}(\text{p},\text{p})^{17}\text{F}$ scattering at $E_{\text{c.m.}}=3$ MeV and the $^{14}\text{O}(\text{la},\text{p})^{17}\text{F}$ reaction rate”, *Phys. Rev. C* **81** (2010) 065802.
- [71] **ALICE** Collaboration, S. Acharya *et al.*, “Measurement of anti- ^3He nuclei absorption in matter and impact on their propagation in the Galaxy”, *Nature Phys.* **19** (2023) 61–71, arXiv:2202.01549 [nucl-ex].
- [72] **ALICE** Collaboration, S. Acharya *et al.*, “Measurement of the low-energy antitriton inelastic cross section”, arXiv:2307.03603 [nucl-ex].
- [73] **ALICE** Collaboration, J. Adam *et al.*, “ $^3_{\Lambda}\text{H}$ and $^3_{\Lambda}\overline{\text{H}}$ production in Pb-Pb collisions at $\sqrt{s_{\text{NN}}} = 2.76$ TeV”, *Phys. Lett. B* **754** (2016) 360–372, arXiv:1506.08453 [nucl-ex].
- [74] **ALICE** Collaboration, S. Acharya *et al.*, “ $^3_{\Lambda}\text{H}$ and $^3_{\Lambda}\overline{\text{H}}$ lifetime measurement in Pb-Pb collisions at $\sqrt{s_{\text{NN}}} = 5.02$ TeV via two-body decay”, *Phys. Lett. B* **797** (2019) 134905, arXiv:1907.06906 [nucl-ex].
- [75] **ALICE** Collaboration, S. Acharya *et al.*, “Hypertriton Production in p-Pb Collisions at $\sqrt{s_{\text{NN}}}=5.02$ TeV”, *Phys. Rev. Lett.* **128** (2022) 252003, arXiv:2107.10627 [nucl-ex].

- [76] **ALICE** Collaboration, S. Acharya *et al.*, “Measurement of the Lifetime and Λ Separation Energy of ${}^3_{\Lambda}\text{H}$ ”, *Phys. Rev. Lett.* **131** (2023) 102302, arXiv:2209.07360 [nucl-ex].
- [77] **ALICE** Collaboration, B. Abelev *et al.*, “Multi-strange baryon production in pp collisions at $\sqrt{s} = 7$ TeV with ALICE”, *Phys. Lett. B* **712** (2012) 309–318, arXiv:1204.0282 [nucl-ex].
- [78] **ALICE** Collaboration, B. B. Abelev *et al.*, “Multi-strange baryon production at mid-rapidity in Pb-Pb collisions at $\sqrt{s_{\text{NN}}} = 2.76$ TeV”, *Phys. Lett. B* **728** (2014) 216–227, arXiv:1307.5543 [nucl-ex]. [Erratum: Phys.Lett.B 734, 409–410 (2014)].
- [79] **ALICE** Collaboration, J. Adam *et al.*, “Multi-strange baryon production in p-Pb collisions at $\sqrt{s_{\text{NN}}} = 5.02$ TeV”, *Phys. Lett. B* **758** (2016) 389–401, arXiv:1512.07227 [nucl-ex].
- [80] T. Chen and C. Guestrin, “Xgboost: A scalable tree boosting system”, in *Proceedings of the 22nd ACM SIGKDD International Conference on Knowledge Discovery and Data Mining*, KDD ’16, p. 785–794. Association for Computing Machinery, New York, NY, USA, 2016.
- [81] K. S. Cranmer, “Kernel estimation in high-energy physics”, *Comput. Phys. Commun.* **136** (2001) 198–207, arXiv:hep-ex/0011057.
- [82] W. Verkerke and D. P. Kirkby, “The RooFit toolkit for data modeling”, *eConf* **C0303241** (2003) MOLT007, arXiv:physics/0306116.
- [83] **ALICE** Collaboration, J. Adam *et al.*, “Quarkonium signal extraction in ALICE”, *ALICE-PUBLIC-2015-006* (2015) . <https://cds.cern.ch/record/2060096/>.
- [84] V. Vovchenko, M. I. Gorenstein, and H. Stoecker, “Finite resonance widths influence the thermal-model description of hadron yields”, *Phys. Rev. C* **98** (2018) 034906, arXiv:1807.02079 [nucl-th].
- [85] **ALICE** Collaboration, “The ALICE experiment – A journey through QCD”, arXiv:2211.04384 [nucl-ex].
- [86] S. Borsanyi, Z. Fodor, J. N. Guenther, R. Kara, S. D. Katz, P. Parotto, A. Pasztor, C. Ratti, and K. K. Szabo, “QCD Crossover at Finite Chemical Potential from Lattice Simulations”, *Phys. Rev. Lett.* **125** (2020) 052001, arXiv:2002.02821 [hep-lat].
- [87] V. Vovchenko, B. Dönigus, and H. Stoecker, “Canonical statistical model analysis of p-p , p -Pb, and Pb-Pb collisions at energies available at the CERN Large Hadron Collider”, *Phys. Rev. C* **100** (2019) 054906, arXiv:1906.03145 [hep-ph].
- [88] J. Cleymans, P. M. Lo, K. Redlich, and N. Sharma, “Multiplicity dependence of (multi)strange baryons in the canonical ensemble with phase shift corrections”, *Phys. Rev. C* **103** (2021) 014904, arXiv:2009.04844 [hep-ph].
- [89] J. Cleymans, H. Oeschler, and K. Redlich, “Statistical model description of K+ and K- production between 1-GeV/A to 10-GeV/A”, *Phys. Lett. B* **485** (2000) 27–31, arXiv:nucl-th/0004025.
- [90] J. D. Brandenburg, N. Lewis, P. Tribedy, and Z. Xu, “Search for baryon junctions in photonuclear processes and isobar collisions at RHIC”, arXiv:2205.05685 [hep-ph].
- [91] E. Schnedermann, J. Sollfrank, and U. W. Heinz, “Thermal phenomenology of hadrons from 200-A/GeV S+S collisions”, *Phys. Rev. C* **48** (1993) 2462–2475, arXiv:nucl-th/9307020.

A Antiparticle-to-particle ratios

A.1 Particle identification of tracked species

The particle identification (PID) of charged pions, protons, ${}^3\text{He}$, and tritons is performed by measuring the specific energy loss (dE/dx) in both the TPC and the ITS, and particle velocity depending on the transverse momentum of the measured particles with the Time-Of-Flight detector (TOF). Due to its electric charge $Z = 2$, ${}^3\text{He}$ is identified using the TPC dE/dx within $|n\sigma^{\text{TPC}}| < 3$, where $n\sigma$ is the deviation of the measured dE/dx from the expected one, normalized to the experimental resolution. A similar approach is applied to protons for $p_T < 1$ GeV/ c after a preliminary $|n\sigma^{\text{ITS}}| < 3$ selection, which is required to reduce the electron contamination. Higher- p_T protons, pions, and tritons are identified using TOF after preliminary TPC PID selections. The $n\sigma^{\text{TPC}}$ or $n\sigma^{\text{TOF}}$ background distributions are fitted outside of the signal window. Their extrapolation within the signal region is integrated to evaluate contaminations due to either misidentified particles or the mismatch of TPC tracks and TOF space points.

A.2 Machine Learning analysis of Ω and ${}^3\Lambda\text{H}$

The Machine Learning (ML) selection of Ω and ${}^3\Lambda\text{H}$ candidates is based on Boosted Decision Trees (BDT). The optimization of the BDT internal parameters is performed using samples of correctly classified signal and background candidates. The signal sample is built from simulated candidates injected on top of a HIJING Pb–Pb event with a Blast-wave p_T distribution [91] derived from the measured production of light flavor hadrons for Ω [45] and of ${}^3\text{He}$ for ${}^3\Lambda\text{H}$ [55]. The background ${}^3\Lambda\text{H}$ candidates are obtained in the data from same-sign combinations of ${}^3\text{He}$ and π tracks. For Ω^- , all the candidates with an invariant-mass deviating more than 7σ from the nominal Ω^- mass are considered as background candidates, with $\sigma \approx 1.7$ MeV/ c^2 being the invariant-mass resolution in the data. The same training variables used in previous analyses are employed for ${}^3\Lambda\text{H}$ [75, 76]: the cosine of the pointing angle $\cos(\theta_p)$ (i.e., the angle between the reconstructed candidate momentum and the straight line connecting the production and decay vertices), the DCA between the decay tracks and the primary vertex (PV), and between the two tracks themselves, the number of TPC space points for the ${}^3\text{He}$ track, and the $n\sigma^{\text{TPC}}$ of the decay tracks. For the Ω^- , the BDT input variables include the DCA of the K^- , π^- and p to the PV, the DCA of the reconstructed Λ to the PV, the minimum distance between the π^- and p , and between the K^- and Λ . The $\cos(\theta_p)$ for both the Ω^- and Λ , and the $n\sigma^{\text{TPC}}$ for p , are also used as BDT input variables. Signal candidates are selected requiring a BDT output score larger than a preset threshold. For ${}^3\Lambda\text{H}$, the threshold is optimized by maximizing the expected signal significance; for the Ω^- , a BDT signal selection efficiency of 50% is required, as it ensures a consistent BDT response in data and MC.

A.3 Systematic uncertainties

The centrality-uncorrelated systematic uncertainty on the yield ratio is obtained as the variance of multiple reanalyses done by varying the tracking and PID selections for π , p , ${}^3\text{He}$, and ${}^3\Lambda\text{H}$, and of the BDT output selections for ${}^3\Lambda\text{H}$ and Ω^- around their nominal values used in the analysis. The background fit function is also changed from exponential to polynomial in the invariant mass fit of ${}^3\Lambda\text{H}$ and Ω^- , while the yields of ${}^3\text{He}$ and ${}^3\Lambda\text{H}$ are alternatively extracted as the integral of a Gaussian fit to the $n\sigma^{\text{TPC}}$ and $n\sigma^{\text{TOF}}$ distributions, respectively. The variations are applied coherently to antiparticles and particles to allow for the cancelation of correlated contributions in the antiparticle-to-particle yield ratios. The MC statistical precision is also considered as a centrality-uncorrelated source of systematic uncertainty. The uncertainty on the material-budget description in MC simulations is correlated with centrality. It is evaluated by varying the amount of material crossed by simulated particles by its uncertainty, estimated to be $\pm 4.5\%$ [49]. The uncertainties on the measured absorption cross sections used to correct the GEANT4 ones are also propagated to the ratios. The consistency of the results obtained with opposite magnetic field polarities is assessed by repeating the measurement separately with the two configurations: a statistically significant discrepancy of about 0.4% and 0.6% due to imperfections in the MC description is

observed in semicentral and central collisions, respectively. The maximum half dispersion between the opposite field polarity results is then assigned as a further centrality-correlated uncertainty. The values of the various contributions are summarised in Table A.1.

Table A.1: Relative systematic uncertainty on the average antiparticle-to-particle ratios due to the different sources considered in the analysis. Only the statistically significant contributions to systematic uncertainties are reported in the table.

Source	$\bar{\Omega}^+/\Omega^-$	π^+/π^-	\bar{p}/p	${}^3\bar{\Lambda}/{}^3\Lambda$	${}^3\bar{H}/{}^3H$	${}^3\bar{He}/{}^3He$
Candidate selection + signal extract.	0.5%	0.05%	0.05%	10%	3%	0.5%
Monte Carlo precision	0.5%	0.1%	0.1%	1%	1%	1%
Material budget	–	0.1%	0.5%	–	–	–
Absorption cross section	–	0.7%	0.5%	1%	10%	1%
Magnetic field polarity	–	0.2–0.3%	0.2–0.3%	–	–	–

A.4 Results for the antiparticle-to-particle ratios

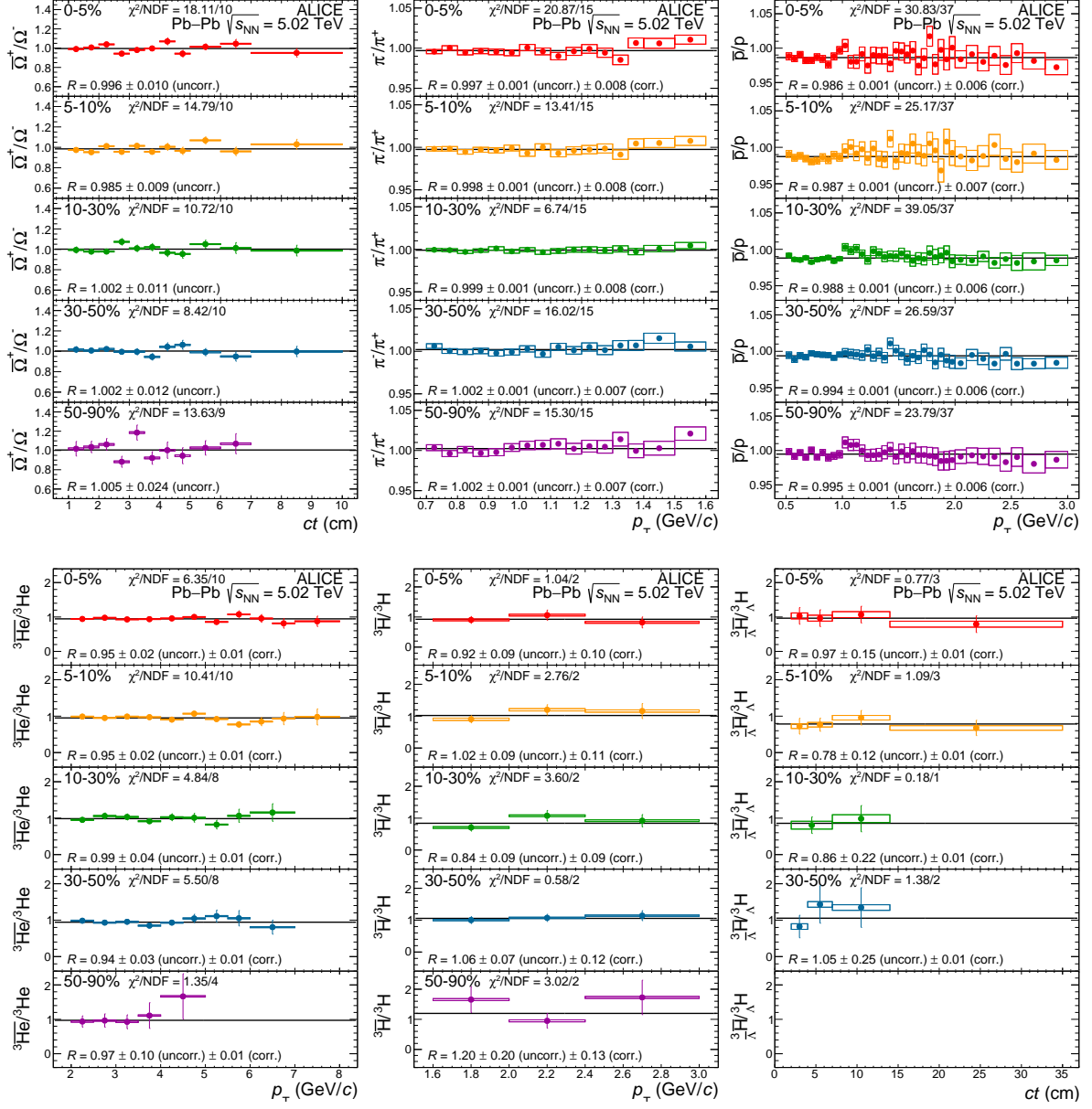


Figure A.1: p_T - and ct -differential ratios of the species used for the chemical potential measurement in the various centrality intervals. Error bars show statistical uncertainties, while boxes represent centrality-uncorrelated uncertainties. The value of R represents the averages weighted with the total uncorrelated uncertainties of the differential measurements. The correlated uncertainties are not shown in the plots.

B Covariance matrices

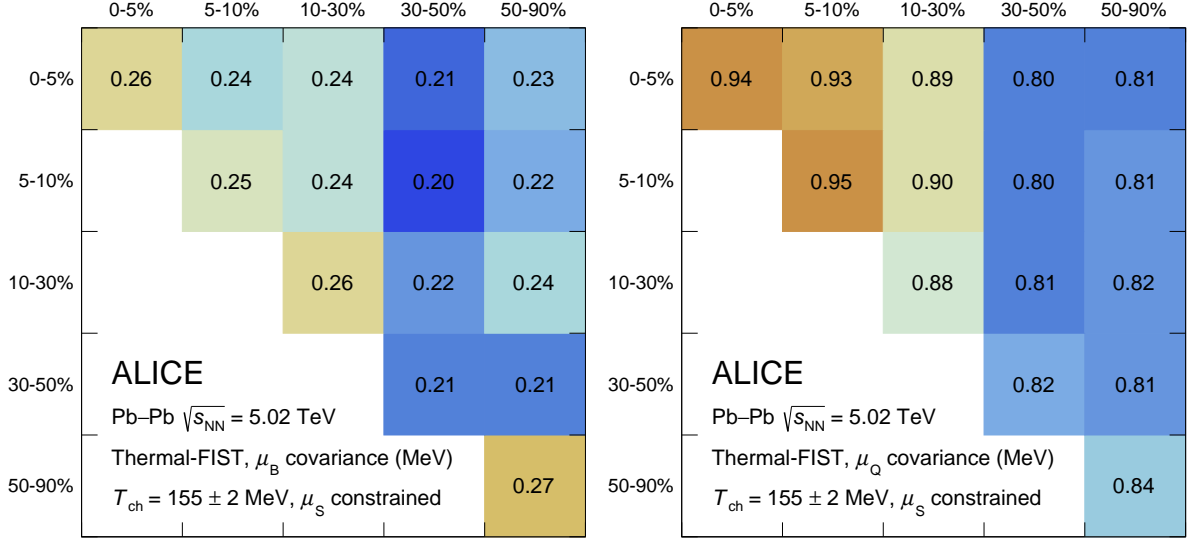


Figure B.1: Covariance matrices of μ_B (left) and μ_Q (right) obtained with Thermal-FIST [22] in the different centrality intervals.

C χ^2 profiles of chemical potential fits

C.1 Thermal-FIST model

Table C.1: Confidence intervals (C.I.) at 1σ , 2σ , and 3σ levels for μ_B and μ_Q .

Observable	1σ C.I. (MeV)	2σ C.I. (MeV)	3σ C.I. (MeV)
μ_B	[0.26, 1.16]	[-0.20, 1.61]	[-0.65, 2.07]
μ_Q	[-1.08, 0.73]	[-1.98, 1.63]	[-2.89, 2.54]

C.2 GSI-Heidelberg model

Table C.2: Confidence intervals (C.I.) at 1σ , 2σ , and 3σ levels for μ_B and μ_Q .

Observable	1σ C.I. (MeV)	2σ C.I. (MeV)	3σ C.I. (MeV)
μ_B	[0.47, 1.33]	[0.05, 1.75]	[-0.38, 2.18]

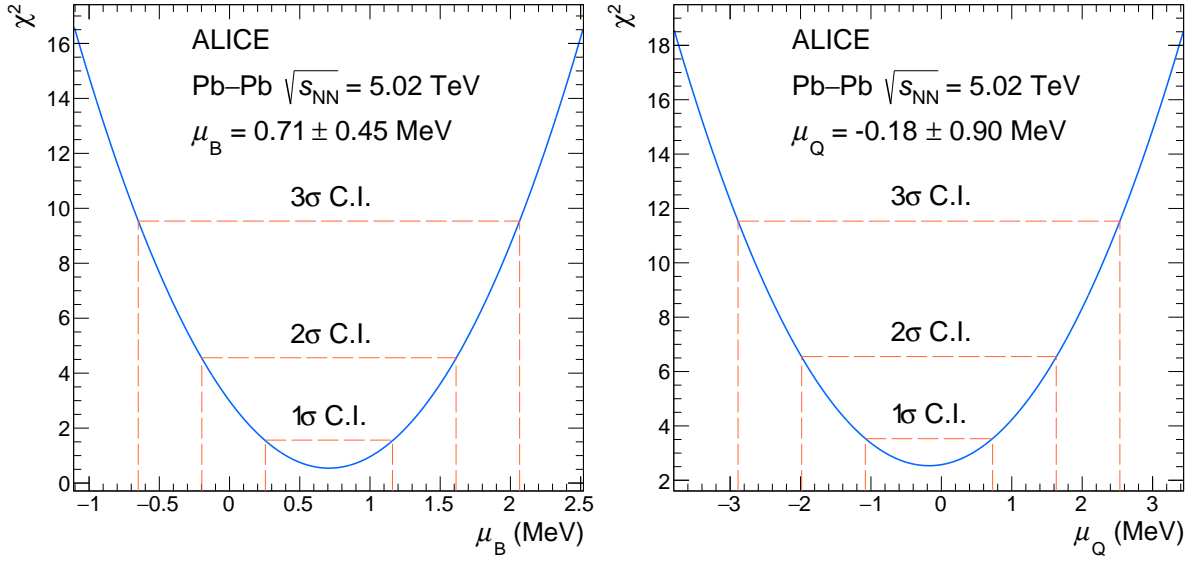


Figure C.1: Profiles of the χ^2 variable minimized in the fit of μ_B (left) and μ_Q (right) obtained with the Thermal-FIST model [22]. The values obtained from the minimization, as well as the 1σ , 2σ , and 3σ confidence intervals, are reported in the figures.

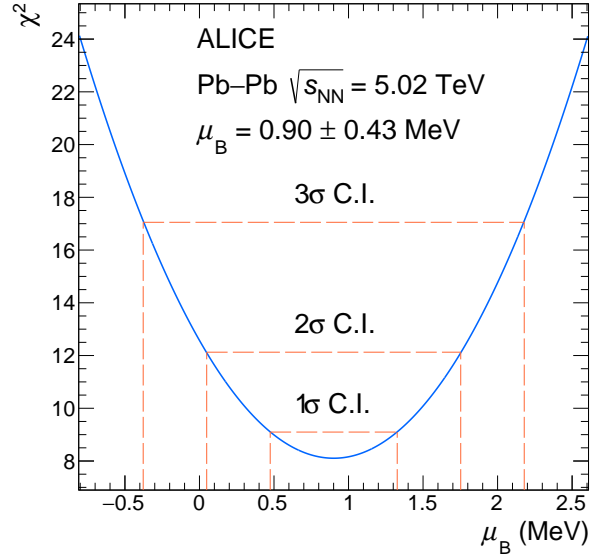


Figure C.2: Profiles of the χ^2 variable minimized in the fit of μ_B obtained with the GSI-Heidelberg model [15, 37, 39]. The values obtained from the minimization, as well as the 1σ , 2σ , and 3σ confidence intervals, are reported in the figures.

D The ALICE Collaboration

S. Acharya ¹²⁷, D. Adamová ⁸⁶, G. Aglieri Rinella ³³, M. Agnello ³⁰, N. Agrawal ²⁶, Z. Ahammed ¹³⁵, S. Ahmad ¹⁶, S.U. Ahn ⁷², I. Ahuja ³⁸, A. Akindinov ¹⁴¹, M. Al-Turany ⁹⁷, D. Aleksandrov ¹⁴¹, B. Alessandro ⁵⁷, H.M. Alfanda ⁶, R. Alfaro Molina ⁶⁸, B. Ali ¹⁶, A. Alici ²⁶, N. Alizadehvandchali ¹¹⁶, A. Alkin ³³, J. Alme ²¹, G. Alocco ⁵³, T. Alt ⁶⁵, A.R. Altamura ⁵¹, I. Altsybeev ⁹⁵, J.R. Alvarado ⁴⁵, M.N. Anaam ⁶, C. Andrei ⁴⁶, N. Andreou ¹¹⁵, A. Andronic ¹²⁶, E. Andronov ¹⁴¹, V. Anguelov ⁹⁴, F. Antinori ⁵⁵, P. Antonioli ⁵², N. Apadula ⁷⁴, L. Aphectche ¹⁰³, H. Appelshäuser ⁶⁵, C. Arata ⁷³, S. Arcelli ²⁶, M. Aresti ²³, R. Arnaldi ⁵⁷, J.G.M.C.A. Arneiro ¹¹⁰, I.C. Arsene ²⁰, M. Arslanok ¹³⁸, A. Augustinus ³³, R. Averbeck ⁹⁷, M.D. Azmi ¹⁶, H. Baba ¹²⁴, A. Badalà ⁵⁴, J. Bae ¹⁰⁴, Y.W. Baek ⁴¹, X. Bai ¹²⁰, R. Bailhache ⁶⁵, Y. Bailung ⁴⁹, R. Bala ⁹¹, A. Balbino ³⁰, A. Baldisseri ¹³⁰, B. Balis ², D. Banerjee ⁴, Z. Banoo ⁹¹, F. Barile ³², L. Barioglio ⁵⁷, M. Barlou ⁷⁸, B. Barman ⁴², G.G. Barnaföldi ⁴⁷, L.S. Barnby ⁸⁵, E. Barreau ¹⁰³, V. Barret ¹²⁷, L. Barreto ¹¹⁰, C. Bartels ¹¹⁹, K. Barth ³³, E. Bartsch ⁶⁵, N. Bastid ¹²⁷, S. Basu ⁷⁵, G. Batigne ¹⁰³, D. Battistini ⁹⁵, B. Batyunya ¹⁴², D. Bauri ⁴⁸, J.L. Bazo Alba ¹⁰¹, I.G. Bearden ⁸³, C. Beattie ¹³⁸, P. Becht ⁹⁷, D. Behera ⁴⁹, I. Belikov ¹²⁹, A.D.C. Bell Hechavarria ¹²⁶, F. Bellini ²⁶, R. Bellwied ¹¹⁶, S. Belokurova ¹⁴¹, L.G.E. Beltran ¹⁰⁹, Y.A.V. Beltran ⁴⁵, G. Bencedi ⁴⁷, S. Beole ²⁵, Y. Berdnikov ¹⁴¹, A. Berdnikova ⁹⁴, L. Bergmann ⁹⁴, M.G. Besoiu ⁶⁴, L. Betev ³³, P.P. Bhaduri ¹³⁵, A. Bhasin ⁹¹, M.A. Bhat ⁴, B. Bhattacharjee ⁴², L. Bianchi ²⁵, N. Bianchi ⁵⁰, J. Bielčík ³⁶, J. Bielčíková ⁸⁶, A.P. Bigot ¹²⁹, A. Bilandzic ⁹⁵, G. Biro ⁴⁷, S. Biswas ⁴, N. Bize ¹⁰³, J.T. Blair ¹⁰⁸, D. Blau ¹⁴¹, M.B. Blidaru ⁹⁷, N. Bluhme ³⁹, C. Blume ⁶⁵, G. Boca ^{22,56}, F. Bock ⁸⁷, T. Bodova ²¹, S. Boi ²³, J. Bok ¹⁷, L. Boldizsár ⁴⁷, M. Bombara ³⁸, P.M. Bond ³³, G. Bonomi ^{134,56}, H. Borel ¹³⁰, A. Borissov ¹⁴¹, A.G. Borquez Carcamo ⁹⁴, H. Bossi ¹³⁸, E. Botta ²⁵, Y.E.M. Bouziani ⁶⁵, L. Bratrud ⁶⁵, P. Braun-Munzinger ⁹⁷, M. Bregant ¹¹⁰, M. Broz ³⁶, G.E. Bruno ^{96,32}, M.D. Buckland ²⁴, D. Budnikov ¹⁴¹, H. Buesching ⁶⁵, S. Bufalino ³⁰, P. Buhler ¹⁰², N. Burmasov ¹⁴¹, Z. Buthelezi ^{69,123}, A. Bylinkin ²¹, S.A. Bysiak ¹⁰⁷, J.C. Cabanillas Noris ¹⁰⁹, M. Cai ⁶, H. Caines ¹³⁸, A. Caliva ²⁹, E. Calvo Villar ¹⁰¹, J.M.M. Camacho ¹⁰⁹, P. Camerini ²⁴, F.D.M. Canedo ¹¹⁰, S.L. Cantway ¹³⁸, M. Carabas ¹¹³, A.A. Carballo ³³, F. Carnesecchi ³³, R. Caron ¹²⁸, L.A.D. Carvalho ¹¹⁰, J. Castillo Castellanos ¹³⁰, F. Catalano ^{33,25}, S. Cattaruzzi ²⁴, C. Ceballos Sanchez ¹⁴², I. Chakaberia ⁷⁴, P. Chakraborty ⁴⁸, S. Chandra ¹³⁵, S. Chapelard ³³, M. Chartier ¹¹⁹, S. Chattopadhyay ¹³⁵, S. Chattopadhyay ⁹⁹, T. Cheng ^{97,6}, C. Cheshkov ¹²⁸, V. Chibante Barroso ³³, D.D. Chinellato ¹¹¹, E.S. Chizzali ^{II,95}, J. Cho ⁵⁹, S. Cho ⁵⁹, P. Chochula ³³, D. Choudhury ⁴², P. Christakoglou ⁸⁴, C.H. Christensen ⁸³, P. Christiansen ⁷⁵, T. Chujo ¹²⁵, M. Ciacco ³⁰, C. Cicalo ⁵³, M.R. Ciupek ⁹⁷, G. Clai^{III,52}, F. Colamaria ⁵¹, J.S. Colburn ¹⁰⁰, D. Colella ^{96,32}, M. Colocci ²⁶, M. Concas ^{IV,33}, G. Conesa Balbastre ⁷³, Z. Conesa del Valle ¹³¹, G. Contin ²⁴, J.G. Contreras ³⁶, M.L. Coquet ¹³⁰, P. Cortese ^{133,57}, M.R. Cosentino ¹¹², F. Costa ³³, S. Costanza ^{22,56}, C. Cot ¹³¹, J. Crkovská ⁹⁴, P. Crochet ¹²⁷, R. Cruz-Torres ⁷⁴, P. Cui ⁶, A. Dainese ⁵⁵, M.C. Danisch ⁹⁴, A. Danu ⁶⁴, P. Das ⁸⁰, P. Das ⁴, S. Das ⁴, A.R. Dash ¹²⁶, S. Dash ⁴⁸, A. De Caro ²⁹, G. de Cataldo ⁵¹, J. de Cuveland ³⁹, A. De Falco ²³, D. De Gruttola ²⁹, N. De Marco ⁵⁷, C. De Martin ²⁴, S. De Pasquale ²⁹, R. Deb ¹³⁴, R. Del Grande ⁹⁵, L. Dello Stritto ^{33,29}, W. Deng ⁶, P. Dhankher ¹⁹, D. Di Bari ³², A. Di Mauro ³³, B. Diab ¹³⁰, R.A. Diaz ^{142,7}, T. Dietel ¹¹⁴, Y. Ding ⁶, J. Ditzel ⁶⁵, R. Divià ³³, D.U. Dixit ¹⁹, Ø. Djuvstrand ²¹, U. Dmitrieva ¹⁴¹, A. Dobrin ⁶⁴, B. Dönigus ⁶⁵, J.M. Dubinski ¹³⁶, A. Dubla ⁹⁷, S. Dudi ⁹⁰, P. Dupieux ¹²⁷, M. Durkac ¹⁰⁶, N. Dzalaiova ¹³, T.M. Eder ¹²⁶, R.J. Ehlers ⁷⁴, F. Eisenhut ⁶⁵, R. Ejima ⁹², D. Elia ⁵¹, B. Erasmus ¹⁰³, F. Ercolelli ²⁶, B. Espagnon ¹³¹, G. Eulisse ³³, D. Evans ¹⁰⁰, S. Evdokimov ¹⁴¹, L. Fabbietti ⁹⁵, M. Faggin ²⁸, J. Faivre ⁷³, F. Fan ⁶, W. Fan ⁷⁴, A. Fantoni ⁵⁰, M. Fasel ⁸⁷, A. Feliciello ⁵⁷, G. Feofilov ¹⁴¹, A. Fernández Téllez ⁴⁵, L. Ferrandi ¹¹⁰, M.B. Ferrer ³³, A. Ferrero ¹³⁰, C. Ferrero ⁵⁷, A. Ferretti ²⁵, V.J.G. Feuillard ⁹⁴, V. Filova ³⁶, D. Finogeev ¹⁴¹, F.M. Fionda ⁵³, E. Flatland ³³, F. Flor ¹¹⁶, A.N. Flores ¹⁰⁸, S. Foertsch ⁶⁹, I. Fokin ⁹⁴, S. Fokin ¹⁴¹, E. Fragiocomo ⁵⁸, E. Frajna ⁴⁷, U. Fuchs ³³, N. Funicello ²⁹, C. Furret ⁷³, A. Furs ¹⁴¹, T. Fusayasu ⁹⁸, J.J. Gaardhøje ⁸³, M. Gagliardi ²⁵, A.M. Gago ¹⁰¹, T. Gahlauf ⁴⁸, C.D. Galvan ¹⁰⁹, D.R. Gangadharan ¹¹⁶, P. Ganoti ⁷⁸, C. Garabatos ⁹⁷, T. García Chávez ⁴⁵, E. Garcia-Solis ⁹, C. Gargiulo ³³, P. Gasik ⁹⁷, A. Gautam ¹¹⁸, M.B. Gay Ducati ⁶⁷, M. Germain ¹⁰³, A. Ghimouz ¹²⁵, C. Ghosh ¹³⁵, M. Giacalone ⁵², G. Gioachin ³⁰, P. Giubellino ^{97,57}, P. Giubilato ²⁸, A.M.C. Glaenzer ¹³⁰, P. Glässel ⁹⁴, E. Glimos ¹²², D.J.Q. Goh ⁷⁶, V. Gonzalez ¹³⁷, P. Gordeev ¹⁴¹, M. Gorgon ², K. Goswami ⁴⁹, S. Gotovac ³⁴, V. Grabski ⁶⁸, L.K. Graczykowski ¹³⁶, E. Grecka ⁸⁶, A. Grelli ⁶⁰, C. Grigoras ³³, V. Grigoriev ¹⁴¹, S. Grigoryan ^{142,1}, F. Grossa ³³, J.F. Grosse-Oetringhaus ³³, R. Grossi ⁹⁷, D. Grund ³⁶, N.A. Grunwald ⁹⁴, G.G. Guardiano ¹¹¹, R. Guernane ⁷³, M. Guilbaud ¹⁰³, K. Gulbrandsen ⁸³, T. Gündem ⁶⁵, T. Gunji ¹²⁴,

- W. Guo ⁶, A. Gupta ⁹¹, R. Gupta ⁴⁹, R. Gupta ¹³⁶, K. Gwizdziel ⁴⁷, L. Gyulai ⁴⁷, C. Hadjidakis ¹³¹, F.U. Haider ⁹¹, S. Haidlova ³⁶, M. Haldar ⁴, H. Hamagaki ⁷⁶, A. Hamdi ⁷⁴, Y. Han ¹³⁹, B.G. Hanley ¹³⁷, R. Hannigan ¹⁰⁸, J. Hansen ⁷⁵, J.W. Harris ¹³⁸, A. Harton ⁹, M.V. Hartung ⁶⁵, H. Hassan ¹¹⁷, D. Hatzifotiadou ⁵², P. Hauer ⁴³, L.B. Havener ¹³⁸, E. Hellbär ⁹⁷, H. Helstrup ³⁵, M. Hemmer ⁶⁵, T. Herman ³⁶, G. Herrera Corral ⁸, F. Herrmann ¹²⁶, S. Herrmann ¹²⁸, K.F. Hetland ³⁵, B. Heybeck ⁶⁵, H. Hillemanns ³³, B. Hippolyte ¹²⁹, F.W. Hoffmann ⁷¹, B. Hofman ⁶⁰, G.H. Hong ¹³⁹, M. Horst ⁹⁵, A. Horzyk ², Y. Hou ⁶, P. Hristov ³³, P. Huhn ⁶⁵, L.M. Huhta ¹¹⁷, T.J. Humanic ⁸⁸, A. Hutson ¹¹⁶, D. Hutter ³⁹, M.C. Hwang ¹⁹, R. Ilkaev ¹⁴¹, H. Ilyas ¹⁴, M. Inaba ¹²⁵, G.M. Innocenti ³³, M. Ippolitov ¹⁴¹, A. Isakov ⁸⁴, T. Isidori ¹¹⁸, M.S. Islam ⁹⁹, M. Ivanov ⁹⁷, M. Ivanov ¹³, V. Ivanov ¹⁴¹, K.E. Iversen ⁷⁵, M. Jablonski ², B. Jacak ^{19,74}, N. Jacazio ²⁶, P.M. Jacobs ⁷⁴, S. Jadlovska ¹⁰⁶, J. Jadlovsky ¹⁰⁶, S. Jaelani ⁸², C. Jahnke ¹¹⁰, M.J. Jakubowska ¹³⁶, M.A. Janik ¹³⁶, T. Janson ⁷¹, S. Ji ¹⁷, S. Jia ¹⁰, A.A.P. Jimenez ⁶⁶, F. Jonas ^{74,87,126}, D.M. Jones ¹¹⁹, J.M. Jowett ^{33,97}, J. Jung ⁶⁵, M. Jung ⁶⁵, A. Junique ³³, A. Jusko ¹⁰⁰, M.J. Kabus ^{33,136}, J. Kaewjai ¹⁰⁵, P. Kalinak ⁶¹, A.S. Kalteyer ⁹⁷, A. Kalweit ³³, D. Karatovic ⁸⁹, O. Karavichev ¹⁴¹, T. Karavicheva ¹⁴¹, P. Karczmarczyk ¹³⁶, E. Karpechev ¹⁴¹, U. Kebschull ⁷¹, R. Keidel ¹⁴⁰, D.L.D. Keijdener ⁶⁰, M. Keil ³³, B. Ketzer ⁴³, S.S. Khade ⁴⁹, A.M. Khan ¹²⁰, S. Khan ¹⁶, A. Khanzadeev ¹⁴¹, Y. Kharlov ¹⁴¹, A. Khatun ¹¹⁸, A. Khuntia ³⁶, Z. Khuranova ⁶⁵, B. Kileng ³⁵, B. Kim ¹⁰⁴, C. Kim ¹⁷, D.J. Kim ¹¹⁷, E.J. Kim ⁷⁰, J. Kim ¹³⁹, J. Kim ⁵⁹, J. Kim ⁷⁰, M. Kim ¹⁹, S. Kim ¹⁸, T. Kim ¹³⁹, K. Kimura ⁹², S. Kirsch ⁶⁵, I. Kisiel ³⁹, S. Kiselev ¹⁴¹, A. Kisiel ¹³⁶, J.P. Kitowski ², J.L. Klay ⁵, J. Klein ³³, S. Klein ⁷⁴, C. Klein-Bösing ¹²⁶, M. Kleiner ⁶⁵, T. Klemenz ⁹⁵, A. Kluge ³³, C. Kobdaj ¹⁰⁵, T. Kollegger ⁹⁷, A. Kondratyev ¹⁴², N. Kondratyeva ¹⁴¹, J. Konig ⁶⁵, S.A. Konigstorfer ⁹⁵, P.J. Konopka ³³, G. Kornakov ¹³⁶, M. Korwieser ⁹⁵, S.D. Koryciak ², A. Kotliarov ⁸⁶, N. Kovacic ⁸⁹, V. Kovalenko ¹⁴¹, M. Kowalski ¹⁰⁷, V. Kozhuharov ³⁷, I. Králik ⁶¹, A. Kravčáková ³⁸, L. Krcal ^{33,39}, M. Krivda ^{100,61}, F. Krizek ⁸⁶, K. Krizkova Gajdosova ³³, M. Kroesen ⁹⁴, M. Krüger ⁶⁵, D.M. Krupova ³⁶, E. Kryshen ¹⁴¹, V. Kučera ⁵⁹, C. Kuhn ¹²⁹, P.G. Kuijer ⁸⁴, T. Kumaoka ¹²⁵, D. Kumar ¹³⁵, L. Kumar ⁹⁰, N. Kumar ⁹⁰, S. Kumar ³², S. Kundu ³³, P. Kurashvili ⁷⁹, A. Kurepin ¹⁴¹, A.B. Kurepin ¹⁴¹, A. Kuryakin ¹⁴¹, S. Kushpil ⁸⁶, V. Kuskov ¹⁴¹, M. Kutyla ¹³⁶, M.J. Kweon ⁵⁹, Y. Kwon ¹³⁹, S.L. La Pointe ³⁹, P. La Rocca ²⁷, A. Lakrathok ¹⁰⁵, M. Lamanna ³³, A.R. Landou ⁷³, R. Langoy ¹²¹, P. Larionov ³³, E. Laudi ³³, L. Lautner ^{33,95}, R. Lavicka ¹⁰², R. Lea ^{134,56}, H. Lee ¹⁰⁴, I. Legrand ⁴⁶, G. Legras ¹²⁶, J. Lehrbach ³⁹, T.M. Lelek ², R.C. Lemmon ⁸⁵, I. León Monzón ¹⁰⁹, M.M. Lesch ⁹⁵, E.D. Lesser ¹⁹, P. Lévai ⁴⁷, X. Li ¹⁰, B.E. Liang-gilman ¹⁹, J. Lien ¹²¹, R. Lietava ¹⁰⁰, I. Likmeta ¹¹⁶, B. Lim ²⁵, S.H. Lim ¹⁷, V. Lindenstruth ³⁹, A. Lindner ⁴⁶, C. Lippmann ⁹⁷, D.H. Liu ⁶, J. Liu ¹¹⁹, G.S.S. Liveraro ¹¹¹, I.M. Lofnes ²¹, C. Loizides ⁸⁷, S. Lokos ¹⁰⁷, J. Lomker ⁶⁰, P. Loncar ³⁴, X. Lopez ¹²⁷, E. López Torres ⁷, P. Lu ^{97,120}, F.V. Lugo ⁶⁸, J.R. Luhder ¹²⁶, M. Lunardon ²⁸, G. Luparello ⁵⁸, Y.G. Ma ⁴⁰, M. Mager ³³, A. Maire ¹²⁹, E.M. Majerz ², M.V. Makariev ³⁷, M. Malaev ¹⁴¹, G. Malfattore ²⁶, N.M. Malik ⁹¹, Q.W. Malik ²⁰, S.K. Malik ⁹¹, L. Malinina ^{I,VII,142}, D. Mallick ¹³¹, N. Mallick ⁴⁹, G. Mandaglio ^{31,54}, S.K. Mandal ⁷⁹, V. Manko ¹⁴¹, F. Manso ¹²⁷, V. Manzari ⁵¹, Y. Mao ⁶, R.W. Marcjan ², G.V. Margagliotti ²⁴, A. Margotti ⁵², A. Marín ⁹⁷, C. Markert ¹⁰⁸, P. Martinengo ³³, M.I. Martínez ⁴⁵, G. Martínez García ¹⁰³, M.P.P. Martins ¹¹⁰, S. Masciocchi ⁹⁷, M. Masera ²⁵, A. Masoni ⁵³, L. Massacrier ¹³¹, O. Massen ⁶⁰, A. Mastroserio ^{132,51}, O. Matonoha ⁷⁵, S. Mattiazzo ²⁸, A. Matyja ¹⁰⁷, C. Mayer ¹⁰⁷, A.L. Mazuecos ³³, F. Mazzaschi ²⁵, M. Mazzilli ³³, J.E. Mdhului ¹²³, Y. Melikyan ⁴⁴, A. Menchaca-Rocha ⁶⁸, J.E.M. Mendez ⁶⁶, E. Meninno ¹⁰², A.S. Menon ¹¹⁶, M. Meres ¹³, Y. Miake ¹²⁵, L. Micheletti ³³, D.L. Mihaylov ⁹⁵, K. Mikhaylov ^{142,141}, D. Miśkowiec ⁹⁷, A. Modak ⁴, B. Mohanty ⁸⁰, M. Mohisin Khan ^{V,16}, M.A. Molander ⁴⁴, S. Monira ¹³⁶, C. Mordasini ¹¹⁷, D.A. Moreira De Godoy ¹²⁶, I. Morozov ¹⁴¹, A. Morsch ³³, T. Mrnjavac ³³, V. Muccifora ⁵⁰, S. Muhuri ¹³⁵, J.D. Mulligan ⁷⁴, A. Mulliri ²³, M.G. Munhoz ¹¹⁰, R.H. Munzer ⁶⁵, H. Murakami ¹²⁴, S. Murray ¹¹⁴, L. Musa ³³, J. Musinsky ⁶¹, J.W. Myrcha ¹³⁶, B. Naik ¹²³, A.I. Nambrath ¹⁹, B.K. Nandi ⁴⁸, R. Nania ⁵², E. Nappi ⁵¹, A.F. Nassirpour ¹⁸, A. Nath ⁹⁴, C. Natrass ¹²², M.N. Naydenov ³⁷, A. Neagu ²⁰, A. Negru ¹¹³, E. Nekrasova ¹⁴¹, L. Nellen ⁶⁶, R. Nepeivoda ⁷⁵, S. Nese ²⁰, G. Neskovic ³⁹, N. Nicassio ⁵¹, B.S. Nielsen ⁸³, E.G. Nielsen ⁸³, S. Nikolaev ¹⁴¹, S. Nikulin ¹⁴¹, V. Nikulin ¹⁴¹, F. Noferini ⁵², S. Noh ¹², P. Nomokonov ¹⁴², J. Norman ¹¹⁹, N. Novitzky ⁸⁷, P. Nowakowski ¹³⁶, A. Nyanin ¹⁴¹, J. Nystrand ²¹, S. Oh ¹⁸, A. Ohlson ⁷⁵, V.A. Okorokov ¹⁴¹, J. Oleniacz ¹³⁶, A. Onnerstad ¹¹⁷, C. Oppedisano ⁵⁷, A. Ortiz Velasquez ⁶⁶, J. Otwinowski ¹⁰⁷, M. Oya ⁹², K. Oyama ⁷⁶, Y. Pachmayer ⁹⁴, S. Padhan ⁴⁸, D. Pagano ^{134,56}, G. Paić ⁶⁶, S. Paisano-Guzmán ⁴⁵, A. Palasciano ⁵¹, S. Panebianco ¹³⁰, H. Park ¹²⁵, H. Park ¹⁰⁴, J. Park ⁵⁹, J.E. Parkkila ³³, Y. Patley ⁴⁸, B. Paul ²³, M.M.D.M. Paulino ¹¹⁰,

H. Pei ⁶, T. Peitzmann ⁶⁰, X. Peng ¹¹, M. Pennisi ²⁵, S. Perciballi ²⁵, D. Peresunko ¹⁴¹, G.M. Perez ⁷, Y. Pestov¹⁴¹, V. Petrov ¹⁴¹, M. Petrovici ⁴⁶, R.P. Pezzi ^{103,67}, S. Piano ⁵⁸, M. Pikna ¹³, P. Pillot ¹⁰³, O. Pinazza ^{52,33}, L. Pinsky ¹¹⁶, C. Pinto ⁹⁵, S. Pisano ⁵⁰, M. Płoskoń ⁷⁴, M. Planinic ⁸⁹, F. Pliquet ⁶⁵, M.G. Poghosyan ⁸⁷, B. Polichtchouk ¹⁴¹, S. Politano ³⁰, N. Poljak ⁸⁹, A. Pop ⁴⁶, S. Porteboeuf-Houssais ¹²⁷, V. Pozdniakov ¹⁴², I.Y. Pozos ⁴⁵, K.K. Pradhan ⁴⁹, S.K. Prasad ⁴, S. Prasad ⁴⁹, R. Preghenella ⁵², F. Prino ⁵⁷, C.A. Pruneau ¹³⁷, I. Pshenichnov ¹⁴¹, M. Puccio ³³, S. Pucillo ²⁵, Z. Pugelova ¹⁰⁶, S. Qiu ⁸⁴, L. Quaglia ²⁵, S. Ragoni ¹⁵, A. Rai ¹³⁸, A. Rakotozafindrabe ¹³⁰, L. Ramello ^{133,57}, F. Rami ¹²⁹, T.A. Rancien ⁷³, M. Rasa ²⁷, S.S. Räsänen ⁴⁴, R. Rath ⁵², M.P. Rauch ²¹, I. Ravasenga ³³, K.F. Read ^{87,122}, C. Reckziegel ¹¹², A.R. Redelbach ³⁹, K. Redlich ^{VI,79}, C.A. Reetz ⁹⁷, H.D. Regules-Medel ⁴⁵, A. Rehman ²¹, F. Reidt ³³, H.A. Reme-Ness ³⁵, Z. Rescakova ³⁸, K. Reygers ⁹⁴, A. Riabov ¹⁴¹, V. Riabov ¹⁴¹, R. Ricci ²⁹, M. Richter ²⁰, A.A. Riedel ⁹⁵, W. Riegler ³³, A.G. Riffero ²⁵, C. Ristea ⁶⁴, M.V. Rodriguez ³³, M. Rodríguez Cahuantzi ⁴⁵, S.A. Rodríguez Ramírez ⁴⁵, K. Røed ²⁰, R. Rogalev ¹⁴¹, E. Rogochaya ¹⁴², T.S. Rogoschinski ⁶⁵, D. Rohr ³³, D. Röhrich ²¹, P.F. Rojas ⁴⁵, S. Rojas Torres ³⁶, P.S. Rokita ¹³⁶, G. Romanenko ²⁶, F. Ronchetti ⁵⁰, A. Rosano ^{31,54}, E.D. Rosas ⁶⁶, K. Roslon ¹³⁶, A. Rossi ⁵⁵, A. Roy ⁴⁹, S. Roy ⁴⁸, N. Rubini ²⁶, D. Ruggiano ¹³⁶, R. Rui ²⁴, P.G. Russek ², R. Russo ⁸⁴, A. Rustamov ⁸¹, E. Ryabinkin ¹⁴¹, Y. Ryabov ¹⁴¹, A. Rybicki ¹⁰⁷, H. Rytkonen ¹¹⁷, J. Ryu ¹⁷, W. Rzesz ¹³⁶, O.A.M. Saarimaki ⁴⁴, S. Sadhu ³², S. Sadovsky ¹⁴¹, J. Saetre ²¹, K. Šafařík ³⁶, P. Saha ⁴², S.K. Saha ⁴, S. Saha ⁸⁰, B. Sahoo ⁴⁹, R. Sahoo ⁴⁹, S. Sahoo ⁶², D. Sahu ⁴⁹, P.K. Sahu ⁶², J. Saini ¹³⁵, K. Sajdakova ³⁸, S. Sakai ¹²⁵, M.P. Salvan ⁹⁷, S. Sambyal ⁹¹, D. Samitz ¹⁰², I. Sanna ^{33,95}, T.B. Saramela ¹¹⁰, D. Sarkar ⁸³, P. Sarma ⁴², V. Sarritzu ²³, V.M. Sarti ⁹⁵, M.H.P. Sas ³³, S. Sawan ⁸⁰, E. Scapparone ⁵², J. Schambach ⁸⁷, H.S. Scheid ⁶⁵, C. Schiaua ⁴⁶, R. Schicker ⁹⁴, F. Schlepper ⁹⁴, A. Schmah ⁹⁷, C. Schmidt ⁹⁷, H.R. Schmidt ⁹³, M.O. Schmidt ³³, M. Schmidt ⁹³, N.V. Schmidt ⁸⁷, A.R. Schmier ¹²², R. Schotter ¹²⁹, A. Schröter ³⁹, J. Schukraft ³³, K. Schweda ⁹⁷, G. Scioli ²⁶, E. Scomparin ⁵⁷, J.E. Seger ¹⁵, Y. Sekiguchi ¹²⁴, D. Sekihata ¹²⁴, M. Selina ⁸⁴, I. Selyuzhenkov ⁹⁷, S. Senyukov ¹²⁹, J.J. Seo ⁹⁴, D. Serebryakov ¹⁴¹, L. Serkin ⁶⁶, L. Šerkšnytė ⁹⁵, A. Sevcenco ⁶⁴, T.J. Shaba ⁶⁹, A. Shabetai ¹⁰³, R. Shahoyan ³³, A. Shangaraev ¹⁴¹, B. Sharma ⁹¹, D. Sharma ⁴⁸, H. Sharma ⁵⁵, M. Sharma ⁹¹, S. Sharma ⁷⁶, S. Sharma ⁹¹, U. Sharma ⁹¹, A. Shatat ¹³¹, O. Sheibani ¹¹⁶, K. Shigaki ⁹², M. Shimomura ⁷⁷, J. Shin ¹², S. Shirinkin ¹⁴¹, Q. Shou ⁴⁰, Y. Sibirski ¹⁴¹, S. Siddhanta ⁵³, T. Siemiaczuk ⁷⁹, T.F. Silva ¹¹⁰, D. Silvermyr ⁷⁵, T. Simantathammakul ¹⁰⁵, R. Simeonov ³⁷, B. Singh ⁹¹, B. Singh ⁹⁵, K. Singh ⁴⁹, R. Singh ⁸⁰, R. Singh ⁹¹, R. Singh ⁴⁹, S. Singh ¹⁶, V.K. Singh ¹³⁵, V. Singhal ¹³⁵, T. Sinha ⁹⁹, B. Sitar ¹³, M. Sitta ^{133,57}, T.B. Skaali ²⁰, G. Skorodumovs ⁹⁴, M. Slupecki ⁴⁴, N. Smirnov ¹³⁸, R.J.M. Snellings ⁶⁰, E.H. Solheim ²⁰, J. Song ¹⁷, C. Sonnabend ^{33,97}, J.M. Sonneveld ⁸⁴, F. Soramel ²⁸, A.B. Soto-hernandez ⁸⁸, R. Spijkers ⁸⁴, I. Sputowska ¹⁰⁷, J. Staa ⁷⁵, J. Stachel ⁹⁴, I. Stan ⁶⁴, P.J. Steffanic ¹²², S.F. Stiefelmaier ⁹⁴, D. Stocco ¹⁰³, I. Storehaug ²⁰, P. Stratmann ¹²⁶, S. Strazzi ²⁶, A. Sturniolo ^{31,54}, C.P. Stylianidis ⁸⁴, A.A.P. Suaide ¹¹⁰, C. Suire ¹³¹, M. Sukhanov ¹⁴¹, M. Suljic ³³, R. Sultanov ¹⁴¹, V. Sumberia ⁹¹, S. Sumowidagdo ⁸², I. Szarka ¹³, M. Szymkowski ¹³⁶, S.F. Taghavi ⁹⁵, G. Taillepied ⁹⁷, J. Takahashi ¹¹¹, G.J. Tambave ⁸⁰, S. Tang ⁶, Z. Tang ¹²⁰, J.D. Tapia Takaki ¹¹⁸, N. Tapus ¹¹³, L.A. Tarasovicova ¹²⁶, M.G. Tarzila ⁴⁶, G.F. Tassielli ³², A. Tauro ³³, A. Tavira García ¹³¹, G. Tejeda Muñoz ⁴⁵, A. Telesca ³³, L. Terlizzi ²⁵, C. Terrevoli ¹¹⁶, S. Thakur ⁴, D. Thomas ¹⁰⁸, A. Tikhonov ¹⁴¹, N. Tiltmann ^{33,126}, A.R. Timmins ¹¹⁶, M. Tkacik ¹⁰⁶, T. Tkacik ¹⁰⁶, A. Toia ⁶⁵, R. Tokumoto ⁹², K. Tomohiro ⁹², N. Topilskaya ¹⁴¹, M. Toppi ⁵⁰, T. Tork ¹³¹, P.V. Torres ⁶⁶, V.V. Torres ¹⁰³, A.G. Torres Ramos ³², A. Trifiró ^{31,54}, A.S. Triolo ^{33,31,54}, S. Tripathy ⁵², T. Tripathy ⁴⁸, S. Trogolo ³³, V. Trubnikov ³, W.H. Trzaska ¹¹⁷, T.P. Trzcinski ¹³⁶, A. Tumkin ¹⁴¹, R. Turrisi ⁵⁵, T.S. Tveter ²⁰, K. Ullaland ²¹, B. Ulukutlu ⁹⁵, A. Uras ¹²⁸, M. Urioni ¹³⁴, G.L. Usai ²³, M. Vala ³⁸, N. Valle ²², L.V.R. van Doremalen ⁶⁰, M. van Leeuwen ⁸⁴, C.A. van Veen ⁹⁴, R.J.G. van Weelden ⁸⁴, P. Vande Vyvre ³³, D. Varga ⁴⁷, Z. Varga ⁴⁷, M. Vasileiou ⁷⁸, A. Vasiliev ¹⁴¹, O. Vázquez Doce ⁵⁰, O. Vazquez Rueda ¹¹⁶, V. Vechernin ¹⁴¹, E. Vercellin ²⁵, S. Vergara Limón ⁴⁵, R. Verma ⁴⁸, L. Vermunt ⁹⁷, R. Vértesi ⁴⁷, M. Verweij ⁶⁰, L. Vickovic ³⁴, Z. Vilakazi ¹²³, O. Villalobos Baillie ¹⁰⁰, A. Villani ²⁴, A. Vinogradov ¹⁴¹, T. Virgili ²⁹, M.M.O. Virta ¹¹⁷, V. Vislavicius ⁷⁵, A. Vodopyanov ¹⁴², B. Volkel ³³, M.A. Völk ⁹⁴, S.A. Voloshin ¹³⁷, G. Volpe ³², B. von Haller ³³, I. Vorobyev ³³, N. Vozniuk ¹⁴¹, J. Vrláková ³⁸, J. Wan ⁴⁰, C. Wang ⁴⁰, D. Wang ⁴⁰, Y. Wang ⁴⁰, Y. Wang ⁶, A. Wegrzynek ³³, F.T. Weiglhofer ³⁹, S.C. Wenzel ³³, J.P. Wessels ¹²⁶, J. Wiechula ⁶⁵, J. Wikne ²⁰, G. Wilk ⁷⁹, J. Wilkinson ⁹⁷, G.A. Willems ¹²⁶, B. Windelband ⁹⁴, M. Winn ¹³⁰, J.R. Wright ¹⁰⁸, W. Wu ⁴⁰, Y. Wu ¹²⁰, R. Xu ⁶, A. Yadav ⁴³, A.K. Yadav ¹³⁵, Y. Yamaguchi ⁹², S. Yang ²¹, S. Yano ⁹², E.R. Yeats ¹⁹, Z. Yin ⁶, I.-K. Yoo ¹⁷, J.H. Yoon ⁵⁹, H. Yu ¹², S. Yuan ²¹, A. Yuncu ⁹⁴, V. Zaccolo ²⁴,

C. Zampolli ³³, F. Zanone ⁹⁴, N. Zardoshti ³³, A. Zarochentsev ¹⁴¹, P. Závada ⁶³, N. Zaviyalov ¹⁴¹, M. Zhalov ¹⁴¹, B. Zhang ⁶, C. Zhang ¹³⁰, L. Zhang ⁴⁰, S. Zhang ⁴⁰, X. Zhang ⁶, Y. Zhang ¹²⁰, Z. Zhang ⁶, M. Zhao ¹⁰, V. Zhrebchevskii ¹⁴¹, Y. Zhi ¹⁰, C. Zhong ⁴⁰, D. Zhou ⁶, Y. Zhou ⁸³, J. Zhu ^{55,6}, Y. Zhu ⁶, S.C. Zugravle ⁵⁷, N. Zurlo ^{134,56}

Affiliation Notes

^I Deceased

^{II} Also at: Max-Planck-Institut für Physik, Munich, Germany

^{III} Also at: Italian National Agency for New Technologies, Energy and Sustainable Economic Development (ENEA), Bologna, Italy

^{IV} Also at: Dipartimento DET del Politecnico di Torino, Turin, Italy

^V Also at: Department of Applied Physics, Aligarh Muslim University, Aligarh, India

^{VI} Also at: Institute of Theoretical Physics, University of Wrocław, Poland

^{VII} Also at: An institution covered by a cooperation agreement with CERN

Collaboration Institutes

¹ A.I. Alikhanyan National Science Laboratory (Yerevan Physics Institute) Foundation, Yerevan, Armenia

² AGH University of Krakow, Cracow, Poland

³ Bogolyubov Institute for Theoretical Physics, National Academy of Sciences of Ukraine, Kiev, Ukraine

⁴ Bose Institute, Department of Physics and Centre for Astroparticle Physics and Space Science (CAPSS), Kolkata, India

⁵ California Polytechnic State University, San Luis Obispo, California, United States

⁶ Central China Normal University, Wuhan, China

⁷ Centro de Aplicaciones Tecnológicas y Desarrollo Nuclear (CEADEN), Havana, Cuba

⁸ Centro de Investigación y de Estudios Avanzados (CINVESTAV), Mexico City and Mérida, Mexico

⁹ Chicago State University, Chicago, Illinois, United States

¹⁰ China Institute of Atomic Energy, Beijing, China

¹¹ China University of Geosciences, Wuhan, China

¹² Chungbuk National University, Cheongju, Republic of Korea

¹³ Comenius University Bratislava, Faculty of Mathematics, Physics and Informatics, Bratislava, Slovak Republic

¹⁴ COMSATS University Islamabad, Islamabad, Pakistan

¹⁵ Creighton University, Omaha, Nebraska, United States

¹⁶ Department of Physics, Aligarh Muslim University, Aligarh, India

¹⁷ Department of Physics, Pusan National University, Pusan, Republic of Korea

¹⁸ Department of Physics, Sejong University, Seoul, Republic of Korea

¹⁹ Department of Physics, University of California, Berkeley, California, United States

²⁰ Department of Physics, University of Oslo, Oslo, Norway

²¹ Department of Physics and Technology, University of Bergen, Bergen, Norway

²² Dipartimento di Fisica, Università di Pavia, Pavia, Italy

²³ Dipartimento di Fisica dell'Università and Sezione INFN, Cagliari, Italy

²⁴ Dipartimento di Fisica dell'Università and Sezione INFN, Trieste, Italy

²⁵ Dipartimento di Fisica dell'Università and Sezione INFN, Turin, Italy

²⁶ Dipartimento di Fisica e Astronomia dell'Università and Sezione INFN, Bologna, Italy

²⁷ Dipartimento di Fisica e Astronomia dell'Università and Sezione INFN, Catania, Italy

²⁸ Dipartimento di Fisica e Astronomia dell'Università and Sezione INFN, Padova, Italy

²⁹ Dipartimento di Fisica ‘E.R. Caianiello’ dell'Università and Gruppo Collegato INFN, Salerno, Italy

³⁰ Dipartimento DISAT del Politecnico and Sezione INFN, Turin, Italy

³¹ Dipartimento di Scienze MIFT, Università di Messina, Messina, Italy

³² Dipartimento Interateneo di Fisica ‘M. Merlin’ and Sezione INFN, Bari, Italy

³³ European Organization for Nuclear Research (CERN), Geneva, Switzerland

³⁴ Faculty of Electrical Engineering, Mechanical Engineering and Naval Architecture, University of Split, Split, Croatia

³⁵ Faculty of Engineering and Science, Western Norway University of Applied Sciences, Bergen, Norway

- ³⁶ Faculty of Nuclear Sciences and Physical Engineering, Czech Technical University in Prague, Prague, Czech Republic
³⁷ Faculty of Physics, Sofia University, Sofia, Bulgaria
³⁸ Faculty of Science, P.J. Šafárik University, Košice, Slovak Republic
³⁹ Frankfurt Institute for Advanced Studies, Johann Wolfgang Goethe-Universität Frankfurt, Frankfurt, Germany
⁴⁰ Fudan University, Shanghai, China
⁴¹ Gangneung-Wonju National University, Gangneung, Republic of Korea
⁴² Gauhati University, Department of Physics, Guwahati, India
⁴³ Helmholtz-Institut für Strahlen- und Kernphysik, Rheinische Friedrich-Wilhelms-Universität Bonn, Bonn, Germany
⁴⁴ Helsinki Institute of Physics (HIP), Helsinki, Finland
⁴⁵ High Energy Physics Group, Universidad Autónoma de Puebla, Puebla, Mexico
⁴⁶ Horia Hulubei National Institute of Physics and Nuclear Engineering, Bucharest, Romania
⁴⁷ HUN-REN Wigner Research Centre for Physics, Budapest, Hungary
⁴⁸ Indian Institute of Technology Bombay (IIT), Mumbai, India
⁴⁹ Indian Institute of Technology Indore, Indore, India
⁵⁰ INFN, Laboratori Nazionali di Frascati, Frascati, Italy
⁵¹ INFN, Sezione di Bari, Bari, Italy
⁵² INFN, Sezione di Bologna, Bologna, Italy
⁵³ INFN, Sezione di Cagliari, Cagliari, Italy
⁵⁴ INFN, Sezione di Catania, Catania, Italy
⁵⁵ INFN, Sezione di Padova, Padova, Italy
⁵⁶ INFN, Sezione di Pavia, Pavia, Italy
⁵⁷ INFN, Sezione di Torino, Turin, Italy
⁵⁸ INFN, Sezione di Trieste, Trieste, Italy
⁵⁹ Inha University, Incheon, Republic of Korea
⁶⁰ Institute for Gravitational and Subatomic Physics (GRASP), Utrecht University/Nikhef, Utrecht, Netherlands
⁶¹ Institute of Experimental Physics, Slovak Academy of Sciences, Košice, Slovak Republic
⁶² Institute of Physics, Homi Bhabha National Institute, Bhubaneswar, India
⁶³ Institute of Physics of the Czech Academy of Sciences, Prague, Czech Republic
⁶⁴ Institute of Space Science (ISS), Bucharest, Romania
⁶⁵ Institut für Kernphysik, Johann Wolfgang Goethe-Universität Frankfurt, Frankfurt, Germany
⁶⁶ Instituto de Ciencias Nucleares, Universidad Nacional Autónoma de México, Mexico City, Mexico
⁶⁷ Instituto de Física, Universidade Federal do Rio Grande do Sul (UFRGS), Porto Alegre, Brazil
⁶⁸ Instituto de Física, Universidad Nacional Autónoma de México, Mexico City, Mexico
⁶⁹ iThemba LABS, National Research Foundation, Somerset West, South Africa
⁷⁰ Jeonbuk National University, Jeonju, Republic of Korea
⁷¹ Johann-Wolfgang-Goethe Universität Frankfurt Institut für Informatik, Fachbereich Informatik und Mathematik, Frankfurt, Germany
⁷² Korea Institute of Science and Technology Information, Daejeon, Republic of Korea
⁷³ Laboratoire de Physique Subatomique et de Cosmologie, Université Grenoble-Alpes, CNRS-IN2P3, Grenoble, France
⁷⁴ Lawrence Berkeley National Laboratory, Berkeley, California, United States
⁷⁵ Lund University Department of Physics, Division of Particle Physics, Lund, Sweden
⁷⁶ Nagasaki Institute of Applied Science, Nagasaki, Japan
⁷⁷ Nara Women's University (NWU), Nara, Japan
⁷⁸ National and Kapodistrian University of Athens, School of Science, Department of Physics , Athens, Greece
⁷⁹ National Centre for Nuclear Research, Warsaw, Poland
⁸⁰ National Institute of Science Education and Research, Homi Bhabha National Institute, Jatni, India
⁸¹ National Nuclear Research Center, Baku, Azerbaijan
⁸² National Research and Innovation Agency - BRIN, Jakarta, Indonesia
⁸³ Niels Bohr Institute, University of Copenhagen, Copenhagen, Denmark
⁸⁴ Nikhef, National institute for subatomic physics, Amsterdam, Netherlands
⁸⁵ Nuclear Physics Group, STFC Daresbury Laboratory, Daresbury, United Kingdom
⁸⁶ Nuclear Physics Institute of the Czech Academy of Sciences, Husinec-Řež, Czech Republic
⁸⁷ Oak Ridge National Laboratory, Oak Ridge, Tennessee, United States

- ⁸⁸ Ohio State University, Columbus, Ohio, United States
⁸⁹ Physics department, Faculty of science, University of Zagreb, Zagreb, Croatia
⁹⁰ Physics Department, Panjab University, Chandigarh, India
⁹¹ Physics Department, University of Jammu, Jammu, India
⁹² Physics Program and International Institute for Sustainability with Knotted Chiral Meta Matter (SKCM2), Hiroshima University, Hiroshima, Japan
⁹³ Physikalisches Institut, Eberhard-Karls-Universität Tübingen, Tübingen, Germany
⁹⁴ Physikalisches Institut, Ruprecht-Karls-Universität Heidelberg, Heidelberg, Germany
⁹⁵ Physik Department, Technische Universität München, Munich, Germany
⁹⁶ Politecnico di Bari and Sezione INFN, Bari, Italy
⁹⁷ Research Division and ExtreMe Matter Institute EMMI, GSI Helmholtzzentrum für Schwerionenforschung GmbH, Darmstadt, Germany
⁹⁸ Saga University, Saga, Japan
⁹⁹ Saha Institute of Nuclear Physics, Homi Bhabha National Institute, Kolkata, India
¹⁰⁰ School of Physics and Astronomy, University of Birmingham, Birmingham, United Kingdom
¹⁰¹ Sección Física, Departamento de Ciencias, Pontificia Universidad Católica del Perú, Lima, Peru
¹⁰² Stefan Meyer Institut für Subatomare Physik (SMI), Vienna, Austria
¹⁰³ SUBATECH, IMT Atlantique, Nantes Université, CNRS-IN2P3, Nantes, France
¹⁰⁴ Sungkyunkwan University, Suwon City, Republic of Korea
¹⁰⁵ Suranaree University of Technology, Nakhon Ratchasima, Thailand
¹⁰⁶ Technical University of Košice, Košice, Slovak Republic
¹⁰⁷ The Henryk Niewodniczanski Institute of Nuclear Physics, Polish Academy of Sciences, Cracow, Poland
¹⁰⁸ The University of Texas at Austin, Austin, Texas, United States
¹⁰⁹ Universidad Autónoma de Sinaloa, Culiacán, Mexico
¹¹⁰ Universidade de São Paulo (USP), São Paulo, Brazil
¹¹¹ Universidade Estadual de Campinas (UNICAMP), Campinas, Brazil
¹¹² Universidade Federal do ABC, Santo Andre, Brazil
¹¹³ Universitatea Națională de Știință și Tehnologie Politehnica Bucuresti, Bucharest, Romania
¹¹⁴ University of Cape Town, Cape Town, South Africa
¹¹⁵ University of Derby, Derby, United Kingdom
¹¹⁶ University of Houston, Houston, Texas, United States
¹¹⁷ University of Jyväskylä, Jyväskylä, Finland
¹¹⁸ University of Kansas, Lawrence, Kansas, United States
¹¹⁹ University of Liverpool, Liverpool, United Kingdom
¹²⁰ University of Science and Technology of China, Hefei, China
¹²¹ University of South-Eastern Norway, Kongsberg, Norway
¹²² University of Tennessee, Knoxville, Tennessee, United States
¹²³ University of the Witwatersrand, Johannesburg, South Africa
¹²⁴ University of Tokyo, Tokyo, Japan
¹²⁵ University of Tsukuba, Tsukuba, Japan
¹²⁶ Universität Münster, Institut für Kernphysik, Münster, Germany
¹²⁷ Université Clermont Auvergne, CNRS/IN2P3, LPC, Clermont-Ferrand, France
¹²⁸ Université de Lyon, CNRS/IN2P3, Institut de Physique des 2 Infinis de Lyon, Lyon, France
¹²⁹ Université de Strasbourg, CNRS, IPHC UMR 7178, F-67000 Strasbourg, France, Strasbourg, France
¹³⁰ Université Paris-Saclay, Centre d'Etudes de Saclay (CEA), IRFU, Département de Physique Nucléaire (DPhN), Saclay, France
¹³¹ Université Paris-Saclay, CNRS/IN2P3, IJCLab, Orsay, France
¹³² Università degli Studi di Foggia, Foggia, Italy
¹³³ Università del Piemonte Orientale, Vercelli, Italy
¹³⁴ Università di Brescia, Brescia, Italy
¹³⁵ Variable Energy Cyclotron Centre, Homi Bhabha National Institute, Kolkata, India
¹³⁶ Warsaw University of Technology, Warsaw, Poland
¹³⁷ Wayne State University, Detroit, Michigan, United States
¹³⁸ Yale University, New Haven, Connecticut, United States
¹³⁹ Yonsei University, Seoul, Republic of Korea
¹⁴⁰ Zentrum für Technologie und Transfer (ZTT), Worms, Germany

¹⁴¹ Affiliated with an institute covered by a cooperation agreement with CERN

¹⁴² Affiliated with an international laboratory covered by a cooperation agreement with CERN.